Stem Cell Reports
Resource
OPEN ACCESS

Efficient Recreation of t(11;22) *EWSR1-FLI1*$^{+}$ in Human Stem Cells Using CRISPR/Cas9

Raul Torres-Ruiz,[1,3,*] Marta Martinez-Lage,[1] Maria C. Martin,[1] Aida Garcia,[2] Clara Bueno,[3] Julio Castaño,[3] Juan C. Ramirez,[4] Pablo Menendez,[3,5,6] Juan C. Cigudosa,[1] and Sandra Rodriguez-Perales[1,*]

[1]Molecular Cytogenetics Group, Human Cancer Genetics Program, Centro Nacional de Investigaciones Oncológicas (CNIO), Madrid 28029, Spain
[2]Hematopoietic Innovative Therapies Division, Centro Investigaciones Energéticas, Medioambientales y Tecnológicas (CIEMAT)-Centro Investigaciones Biomédicas Red Enfermedades Raras (CIBERER), Madrid 28040, Spain
[3]Department of Biomedicine, Josep Carreras Leukemia Research Institute, School of Medicine, University of Barcelona, Barcelona 08036, Spain
[4]VIVEBioTECH, San Sebastian 20009, Spain
[5]Institució Catalana de Recerca i Estudis Avançats (ICREA), Passeig Lluis Companys
[6]Centro de Investigación Biomédica en Red de Cáncer (CIBER-ONC), ISCIII
Barcelona 08010, Spain
*Correspondence: rtorresr@cnio.es (R.T.-R.), srodriguezp@cnio.es (S.R.-P.)
http://dx.doi.org/10.1016/j.stemcr.2017.04.014

SUMMARY

Efficient methodologies for recreating cancer-associated chromosome translocations are in high demand as tools for investigating how such events initiate cancer. The CRISPR/Cas9 system has been used to reconstruct the genetics of these complex rearrangements at native loci while maintaining the architecture and regulatory elements. However, the CRISPR system remains inefficient in human stem cells. Here, we compared three strategies aimed at enhancing the efficiency of the CRISPR-mediated t(11;22) translocation in human stem cells, including mesenchymal and induced pluripotent stem cells: (1) using end-joining DNA processing factors involved in repair mechanisms, or (2) ssODNs to guide the ligation of the double-strand break ends generated by CRISPR/Cas9; and (3) all-in-one plasmid or ribonucleoprotein complex-based approaches. We report that the generation of targeted t(11;22) is significantly increased by using a combination of ribonucleoprotein complexes and ssODNs. The CRISPR/Cas9-mediated generation of targeted t(11;22) in human stem cells opens up new avenues in modeling Ewing sarcoma.

INTRODUCTION

Chromosome translocations are common genomic events in cancer and are the initiating event in many leukemias and sarcomas (http://cgap.nci.nih.gov/Chromosomes/Mitelman). Cancer-associated chromosomal translocations generate novel chromosomes, placing genes in new linkage relationships that can result in the generation of fusion genes or the overexpression of proto-oncogenes. Given their contribution to cancer pathogenesis, chromosomal translocations have been widely studied to better understand the mechanisms involved in their formation and the downstream molecular consequences (Chen et al., 2010; Guryanova and Levine, 2013; Rodriguez-Perales et al., 2015). Genetically modified cells and animal models are essential tools for studying both the function of chromosomal translocations and the initiating oncogenic events in cancer. Targeted chromosomal translocations have been generated de novo in human and mouse models using technologies based on P1 Cre-*loxP* (Forster et al., 2005; Van Deursen et al., 1995), zinc-finger nucleases (ZFN) (Brunet et al., 2009), and transcription activator-like effector nucleases (TALENs) (Piganeau et al., 2013); these approaches generate two derivative chromosomes while maintaining the spatial architecture and regulatory elements of the genomic rearrangement.

The prokaryotic clustered regularly interspaced short palindromic repeats (CRISPR)/Cas9 system (Jinek et al., 2012) has been adapted to induce specific double-strand breaks (DSBs) in the genomes of many species (Cong et al., 2013; Mali et al., 2013). This technology has facilitated and accelerated genome engineering through the targeting of specific locations in the genome guided by single-guide RNA (sgRNA) (Jinek et al., 2012). A key advantage of the CRISPR/Cas9 genome editing over more traditional gene-targeting strategies is its high efficiency, which renders common selection procedures unnecessary (Li et al., 2014; Yang et al., 2013). The CRISPR/Cas9 system was recently adapted to induce chromosomal translocations in vitro (Torres et al., 2014b) and in vivo in mouse models (Blasco et al., 2014; Maddalo et al., 2014). These approaches were based in the simultaneous use of two sgRNAs, resulting in two targeted DSBs that when resolved by the DNA repair machinery can generate specific chromosomal translocations. However, although CRISPR/Cas9 technology considerably increases the efficiency of chromosomal translocations, identification of a bona fide targeted clone requires screening of many clones, especially with stem cells.

Cancer is generally studied after the transformation events are completed, and patient samples are therefore not amenable to analysis of the mechanisms through which cancer-specific chromosomal translocations initiate

oncogenesis. CRISPR/Cas9 genome editing has thus emerged as a tool with enormous potential for assisting in the generation of in vitro and in vivo cancer models, and its combination with human embryonic or adult stem cells will likely prove invaluable for studying the molecular and cellular origin of human disease. However, making this approach feasible requires alternatives to increase the specificity and efficiency of genome targeting in human stem cells.

Here we have compared three strategies for enhancing the efficiency of CRISPR/Cas9-mediated chromosomal translocations in human stem cells, including mesenchymal stem cells (hMSCs) and induced pluripotent stem cells (hiPSCs): (1) promoting chromosomal translocations with end-joining DNA processing factors involved in classical non-homologous end-joining (cNHEJ) and alternative end-joining (altNHEJ); (2) using single-stranded oligodeoxynucleotides (ssODNs) to guide the ligation of DSB ends generated by CRISPR/Cas9; and (3) all-in-one plasmid or ribonucleoprotein (RNP) complex-based approaches. We report that targeted chromosomal translocations are generated more efficiently when the all-in-one plasmid, RNP complex, and ssODN-based approaches are used, with the most efficient strategy being the combination of RNP complexes with translocation-ssODNs. These results represent a significant technical advance toward the induction of targeted chromosomal translocations in human stem cells.

RESULTS

The *All-in-One* Plasmid Increases Genome-Editing Efficiency

The CRISPR/Cas9 system was adapted to induce targeted chromosomal translocations using a two-plasmid approach for the co-expression of two sgRNAs (pLVX-sgRNA$^{\#1}$-Cas9 and pLVX-sgRNA$^{\#2}$-Cas9) (Torres et al., 2014b). Although this approach allows for efficient generation of chromosomal translocations in easy-to-transfect cell lines, the recreation of such translocations in human stem cells remains a challenge. Thus, improved methods need to be developed to increase the specificity and efficiency of genome targeting in human stem cells. To maximize the concurrent cellular delivery of CRISPR components, we established a Cas9 *all-in-one* expression plasmid (pLVX-U6-sgRNA$^{\#1}$-H1-sgRNA$^{\#2}$-Cas9-2A-eGFP; hereafter pLV-U6$^{\#1}$H1$^{\#2}$-C9G) (Figure 1A) that drives similar sgRNA expression levels from two different RNA polymerase III promoters (U6 and H1) and a simultaneously regulated expression of Cas9 and GFP proteins by a 2A self-cleaving peptide. As a test model we focused on the t(11;22)(q24;q12) chromosomal translocation, a hallmark of Ewing sarcoma believed to occur in hMSCs (Delattre et al., 1994). Transfection optimization assays first showed that nucleofection, an electroporation-based transfection method, is the most efficient delivery approach for hMSCs, and an extremely robust transfection approach for HEK293 cells (Figure S1). Thus, HEK293 cells and hMSCs were nucleofected with pLVX-sgRNA$^{\#1}$-Cas9 plus pLVX-sgRNA$^{\#2}$-Cas9 or with pLV-U6$^{\#1}$H1$^{\#2}$-C9G (2 μg of plasmid), and DNA was isolated after 72 hr for analysis of the chromosomal translocation involving *EWSR1* and *FLI1* loci. The t(11;22)(q24;q12) translocation was successfully reproduced in both HEK293 cells and hMSCs (Figure 1B). Fluorescence in situ hybridization (FISH) assays using dual-fusion probes 48–72 hr after transfection revealed significantly higher levels of targeted chromosomal translocations with the *all-in-one* vector than with the two-plasmid system (2.1-fold [from 0.48% to 1.04%] in HEK293 and 6.5-fold [from 0.11% to 0.68%] in hMSCs) (Figure 1C and Table S1). The presence of the balanced translocation at the genome level was confirmed by junction genomic PCR and Sanger sequencing (Figures 1D and S2). Importantly, RT-PCR confirmed the expression of both derivative fusion genes *EWSR1-FLI1* and *FLI1-EWSR1* (Figure S2B). Similarly, the fusion protein was detected by western blot using a human anti-FLI1 antibody (Figure S2C). The increased frequency of t(11;22)(q24;q12) targeted cells when the pLV-U6$^{\#1}$H1$^{\#2}$-C9G construct was used was not associated with off-target effects at the predicted top off-target sites (http://crispr.mit.edu/ and https://benchling.com/) as determined by T7 endonuclease assay (Figure S3). The pLV-U6$^{\#1}$H1$^{\#2}$-C9G plasmid drives co-expression of EGFP linked to Cas9 via a 2A peptide, enabling fluorescence-activated cell sorting (FACS) selection of transfected cells. We thus determined the frequency of t(11;22) targeted cells within the EGFP^{+} population of hMSCs FACS-purified 72 hr after nucleofection. FISH assays revealed that EGFP^{+} hMSCs nucleofected with the *all-in-one* vector had a 3.8-fold higher rate of targeted t(11;22) (from 0.22 to 0.83%) than unsorted hMSCs (Figures 2A and 2B; Table S1). To test the influence of plasmid load on the induction of t(11;22) translocation, we sorted transfected HEK293 cells, based on EGFP expression levels, into eGFP^{high} and eGFP^{low} populations 72 hr after nucleofection (Figure 2C). HEK293 eGFP^{high} cells had a 2.3-fold higher translocation rate than unsorted cells (from 0.77% to 1.73%), whereas eGFP^{low} cells showed no significant increase (from 0.77 to 0.45%) (Figure 2D and Table S1). Collectively, the pLV-U6$^{\#1}$H1$^{\#2}$-C9G construct coupled with FACS selection of transfected cells yields significantly higher targeted t(11;22) translocation rates in HEK293 and hMSCs than those achieved with the two-plasmid system (Torres et al., 2014b).

To further improve the all-in-one approach, we incorporated a second nuclear localization signal (NLS) at the 5′

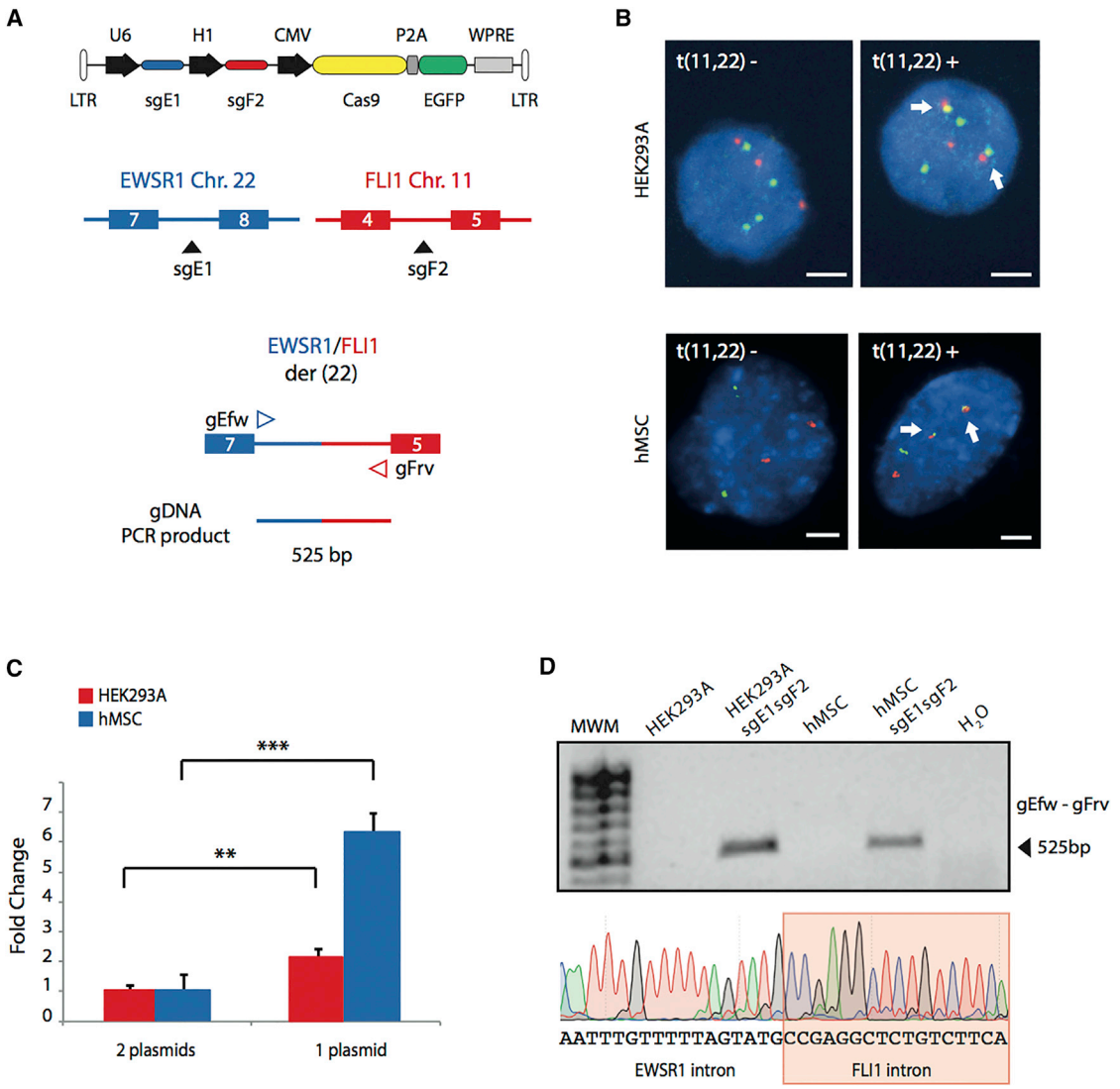

Figure 1. Validation of the *All-in-One* Cas9 CRIPSR Plasmid in HEK293 and hMSCs

(A) pLV-U6sgRNA$^{\#1}$-H1sgRNA$^{\#2}$-C9G *all-in-one* plasmid co-expressing sgRNAs targeting introns in EWSR1 (sgE1) and FLI1 (sgF2) and expressing Cas9 protein. The middle schemes show the location of the regions targeted by sgE1 and sgF2 sgRNAs in the t(11;22)/*EWSR1-FLI1* chromosomal translocation: *EWSR1* intron 7 (sgE1) and *FLI1* intron 4 (sgF2). The lower schemes show PCR oligonucleotide positions and PCR product sizes. The U6, H1, and CMV promoters are represented as black arrows. LTR, long terminal repeat; P2A, 2A self-cleaving peptide; EGFP, enhanced green fluorescent protein; WPRE, woodchuck post-transcriptional regulatory element.

(B) Representative FISH images obtained with a dual-color dual-fusion probe (*EWSR1* in green and *FLI1* in red), showing HEK293 and hMSCs positive and negative for t(11;22). Arrows indicate fusion signals corresponding to the junction regions. Interphase nuclei are counterstained with DAPI. Scale bars, 10 μm.

(C) Fold change in the number of FISH-identified t(11;22)$^{+}$ HEK293 and hMSCs obtained using the all-in-one plasmid approach (one plasmid) versus the two-plasmid approach. Data are means ± SEM (n = 3 independent experiments); **p < 0.01, ***p < 0.001, unpaired Student's t test.

(D) Top: agarose gel electrophoresis of translocation-specific PCR products from pooled HEK293 and hMSC samples. Bottom: representative Sanger sequencing chromatogram showing the breakpoint region in the *EWSR1-FLI1* fusion gene mapped at der(22) in hMSCs.

end of the Cas9 coding region of the pLV-U6$^{\#1}$H1$^{\#2}$-C9G plasmid (Figure S4A). Immunofluorescence microscopy showed that this additional NLS increases nuclear uptake of Cas9 in HEK293 and hMSCs and subsequent genome-engineering activity (Figure 3A). Analysis of the nucleoplasm/cytoplasm fluorescence ratio further supported

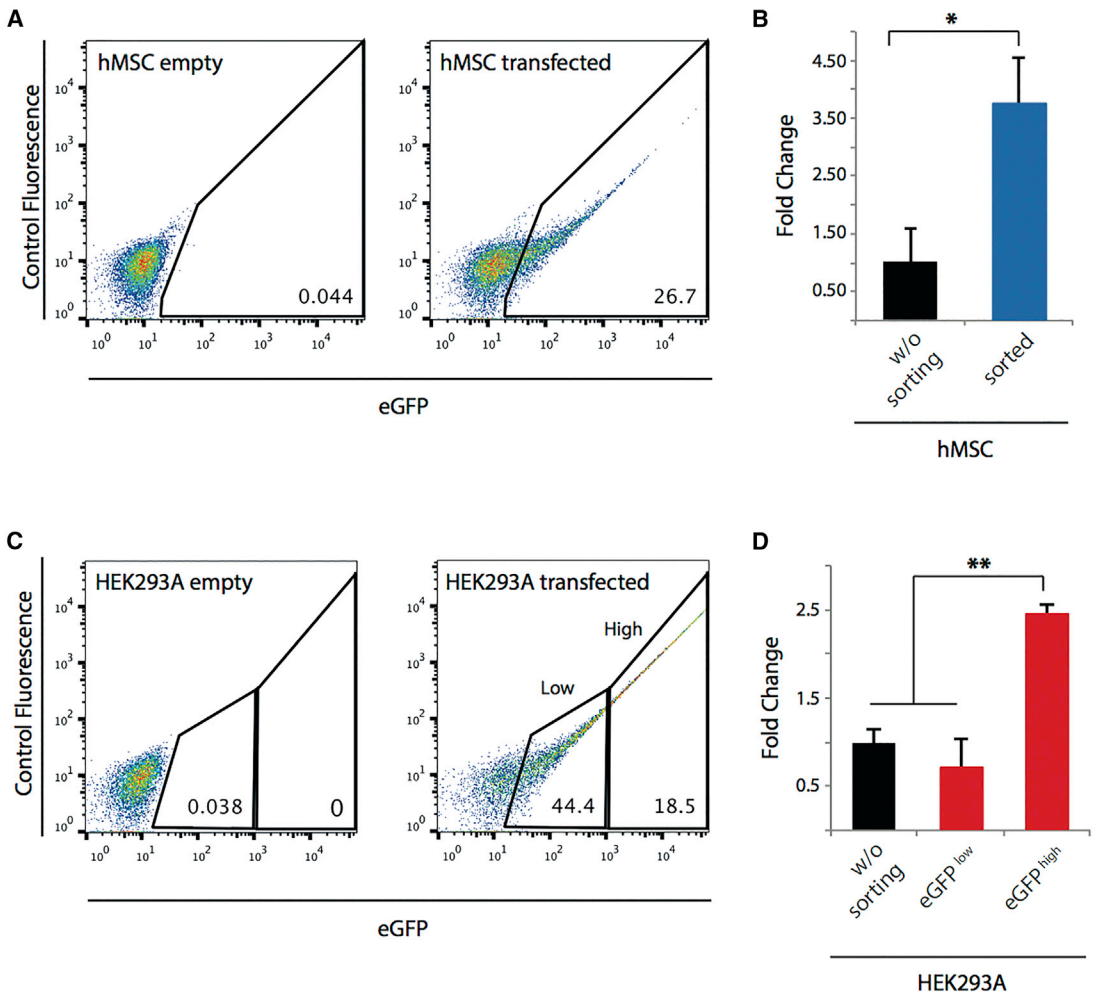

Figure 2. FACS Sorting of Cas9-2A-GFP-Transfected Cells Enriches for Efficiently Engineered t(11;22) Translocations

(A) Representative EGFP flow cytometry profiles for transfected hMSCs. The percentages of $EGFP^{+}$ cells in the initial population are indicated.

(B) Fold-change variation in the number of engineered t(11;22) translocations determined by FISH in hMSCs with or without GFP FACS purification. Data are means ± SEM (n = 3 independent experiments); *p < 0.05.

(C) Representative EGFP flow-cytometry profiles for transfected HEK293 cells. The percentages of GFP^{low} and GFP^{high} cells in the initial population are indicated.

(D) Fold-change variation in the number of engineered t(11;22) translocations evaluated by FISH in HEK293 cells without or with sorting of either GFP^{low} and GFP^{high} cells. Data are means ± SEM (n = 3 independent experiments); **p < 0.01, unpaired Student's t test.

that an extra NLS increases the nuclear localization of the Cas9 (Figure 3B). Western blot confirmed similar expression of Cas9 protein in both 1xNLS and 2xNLS conditions (Figure S4B). On-target T7 endonuclease analysis of cells edited with pLV-$U6^{\#1}H1^{\#2}$-C9G and sgRNA-F2 revealed that 2xNLS Cas9 plasmid increases the rate of genomic cleavage 12-fold (from 3.3% to 37.2%) (Figure 3C). FISH analysis revealed that the 2xNLS version of pLV-$U6^{\#1}H1^{\#2}$-C9G significantly increased the frequency of cells harboring the t(11;22) translocation 3.6-fold in HEK293 cells (from 0.50% to 1.83%) and 7.1-fold in hMSCs (from 0.06% to 0.46%) (Figure 3D and Table S1). The high percentage of indel formation (37.2%) at the on-target site revealed that NHEJ is still more efficient at rejoining the DSBs of the broken ends than at generating chromosomal translocations.

Guided Rejoining of DSB by ssODN Donor Templates Enhances Targeted Generation of t(11;22) Translocation

The high rate of rejoining at the *EWSR1* and *FLI1* target sites without induction of translocation prompted us to

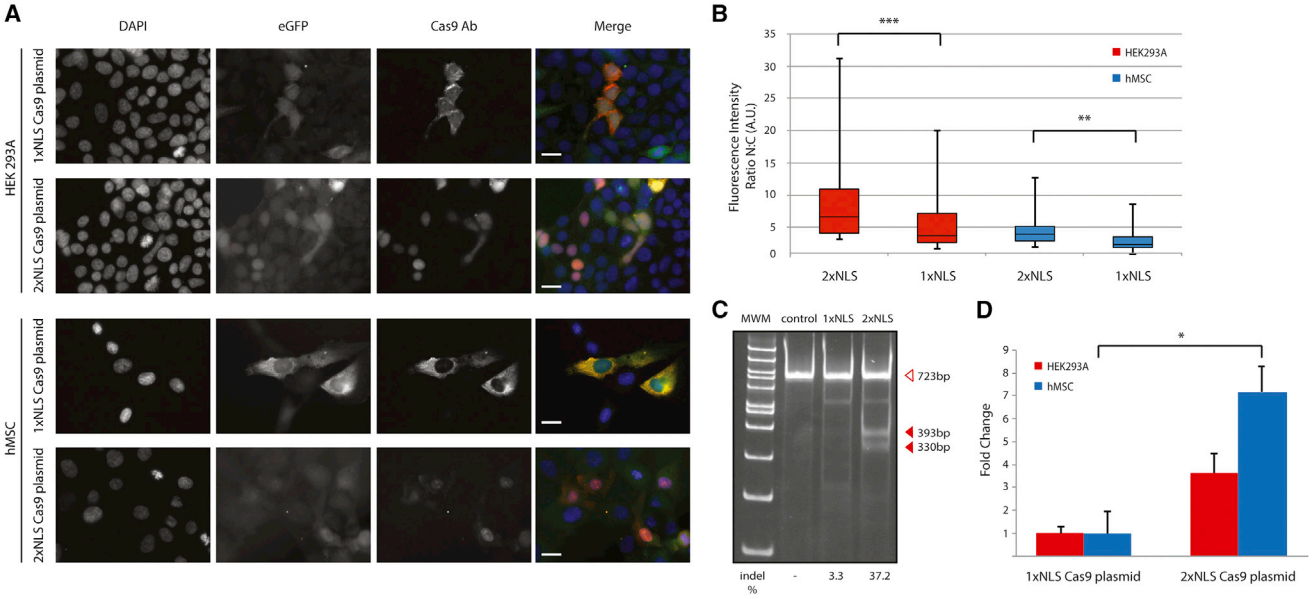

Figure 3. Effect of Nuclear Localization Signals on Cas9 Protein Function

(A) Representative immunofluorescence images of HEK293 and hMSCs transfected with constructs encoding nuclear localization signal (1xNLS or 2xNLS) versions of pLV-U6#1H1#2-C9G stained with anti-Cas9 antibody to visualize Cas9 localization. DNA was counterstained with DAPI. Scale bar, 50 μm.

(B) Nuclear/cytoplasm ratio of Cas9 with 1xNLS or 2xNLS signals. n, number of analyzed cells. Data are means ± SEM; **p < 0.01, ***p < 0.001, unpaired Student's t test.

(C) Representative sgF2 T7 endonuclease I assay in HEK293 cells to determine the targeting activity of 1xNLS or 2xNLS versions of pLV-U6$^{\#1}$H1$^{\#2}$-C9G. Cells were either transfected with an empty pLV-U6H1-C9G plasmid (control) or with 1xNLS-pLV-U6#1H1#2-C9G or 2xNLS-pLV-U6#1H1#2-C9G plasmids. Open triangle depicts the full-length PCR product and filled triangles the digestion products.

(D) Fold-change variation in the number of engineered t(11;22) translocations evaluated by FISH in HEK293 cells and hMSCs transfected with 1xNLS versus 2xNLS versions of pLV-U6$^{\#1}$H1$^{\#2}$-C9G vector. Data are means ± SEM (n = 3 independent experiments); *p < 0.05, unpaired Student's t test.

investigate ways to further promote the t(11;22) translocation. Targeted integration or large deletions can be achieved by combining the CRISPR system with ssODN templates containing homology arms flanking the genomic modification site (Yoshimi et al., 2016). To facilitate the genomic translocation, we designed *translocation*-ssODN donors, hypothesizing that ssODNs would guide homologous-directed (HDR) rejoining of the translocation-derived chromosomes. We generated five different-length ssODNs (60–180 nt), each carrying the 5′ and 3′ portions complementary to the upstream and downstream regions of the der(22) derivative chromosome breakpoint (Figure 4A; nucleotide sequences are shown in Table S2). HEK293 cells were nucleofected with 2 μg of the pLV-U6$^{\#1}$H1$^{\#2}$-C9G-2NLS *all-in-one* CRISPR vector and 200 pmol of *translocation*-ssODN donor. FISH analysis of translocation-editing efficiency 72 hr after nucleofection confirmed that co-nucleofection with ssODNs increased translocation frequency by 2- to 10-fold (from 0.11% to 1.11%) (Figure 4B). The highest increase was achieved with the 150-nt ssODN, with longer and shorter ssODNs being less efficient (Figure 4B and Table S1). We next tested the combined use of two 150-nt *translocation*-ssODN donors, one for each derivative chromosome. Delivery into HEK293 cells of two *translocation*-ssODNs yielded limited improvement in translocation frequency over that achieved with a single ssODN (from 1.24% to 1.57% to 2.02%) (Figure 4C). However, delivery of two *translocation*-ssODNs to hMSCs produced an 11-fold increase in the translocation frequency compared with absence of ssODN (from 0.27% to 2.67%) (Figure 4D and Table S1), suggesting that two *translocation*-ssODN donors, one for each derivative chromosome, enhance the frequency of t(11;22) in stem cells.

Co-transduction with End-Joining DNA-Processing Factors Enhances Targeted Generation of the t(11;22) Translocation in hMSCs

Targeted gene disruption can be increased by co-transfection with DNA end-processing enzymes (Certo et al., 2012), and the DNA end-joining mechanism influences the efficiency of translocation generation. To study the

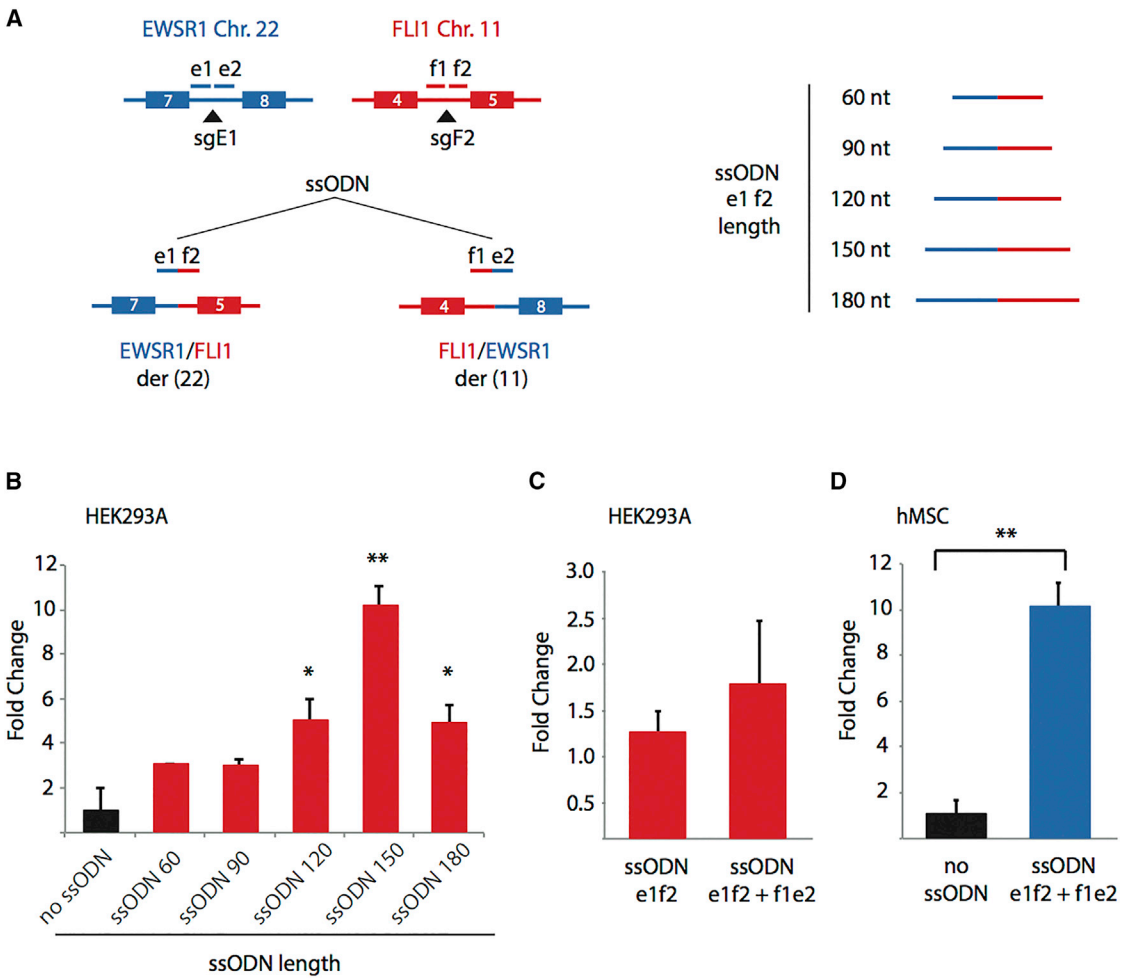

Figure 4. Contribution of ssODNs and DNA End-Processing Factors to CRISPR/Cas9 Targeting Efficiency

(A) ssODN strategy, indicating the sgRNA target loci and the e1f2 and f1e2 ssODNs flanking the breakpoint regions mapping to introns in *FLI1* (red) and *EWSR1* (blue). The scheme on the right represents the lengths of the e1f2 ssODNs.

(B) Influence of ssODN length on the efficiency of t(11;22) translocations in HEK293 cells evaluated by FISH.

(C and D) FISH evaluation of the influence of two ssODNs versus one ssODN on the efficiency of t(11;22) generation in HEK293 cells (C) and without ssODNs versus two ssODNs in hMSCs (D).

Data are means ± SEM (n = 3 independent experiments); *p < 0.05, **p < 0.01, unpaired Student's t test.

ability of different DNA end-joining factors to promote CRISPR-targeted translocations in the rejoining of the CRISPR-induced DSBs, we ectopically expressed genes involved in classical or alternative NHEJ repair. HEK293 cells and hMSCs were both co-nucleofected with the pLV-U6$^{\#1}$H1$^{\#2}$-C9G-2xNLS *all-in-one* CRISPR plasmid and a vector driving expression of one of the following end-joining DNA processing factors: *AICDA*, *ARTEMIS*, *DCLREI*, *FEN1*, *MRE11*, *TREX2*, or *PARP1*. FISH analysis showed that none of these factors had a substantial effect on translocation generation in HEK293 cells (Figure 5A). However, TREX2 and PARP1 induced a 2.2-fold increase in targeted translocations in hMSCs (from 0.33% to 0.72% or 0.73%, respectively) (Figure 5B and Table S1). Importantly, overexpression of end-processing factors did not induce cell toxicity (data not shown).

Cas9 Ribonucleoproteins Robustly Enhance Targeted t(11;22) Translocation in hMSCs

Recent studies in a variety of human stem cells have demonstrated that recombinant Cas9 protein can be efficiently delivered by electroporation or nucleofection (Chen et al., 2013; Gaj et al., 2012; Kim et al., 2014; Liu et al., 2015; Ramakrishna et al., 2014). Moreover, the use of Cas9 RNPs (purified recombinant Cas9 protein complexed with an in vitro transcribed sgRNA) further

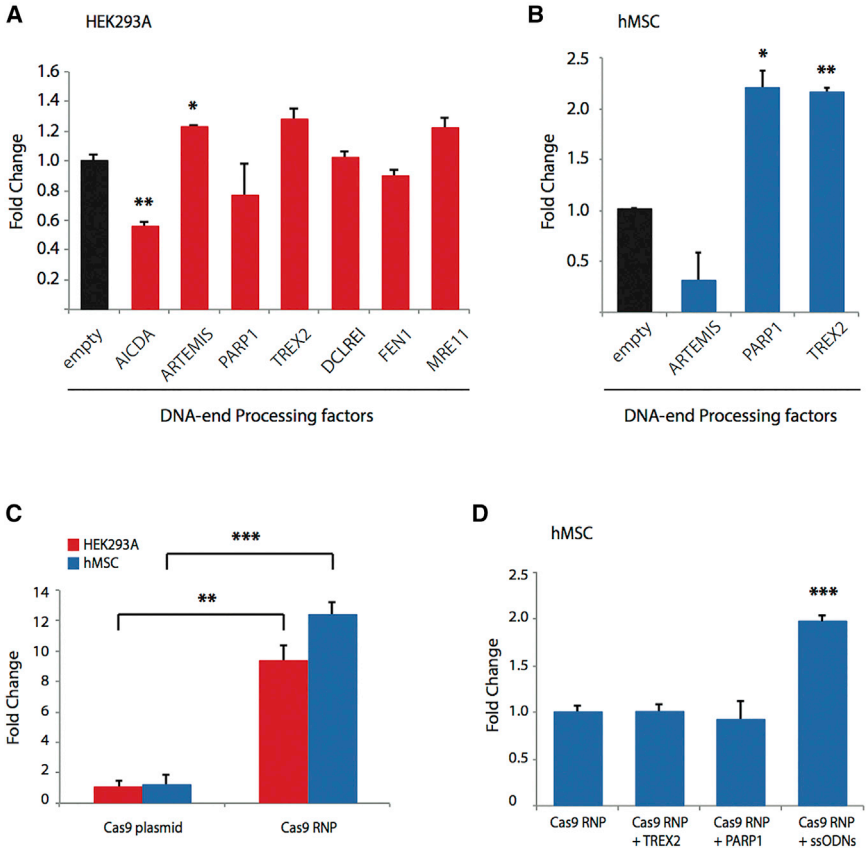

Figure 5. Contribution of DNA End-Processing Factors and RNPs to CRISPR/Cas9-Mediated t(11;22) Generation

(A and B) Influence of different DNA end-processing factors on the efficiency of t(11;22) translocation in HEK293 cells (A) and hMSCs (B).

(C) FISH evaluation of the frequency of t(11;22) translocations engineered with 3xNLS RNP complexes in HEK293 cells and hMSCs.

(D) Frequency of engineered t(11;22) translocations evaluated by FISH in hMSCs transfected with Cas9 RNP, ssODNs, and TREX2 and PARP1 factors.

Data are means ± SEM (n = 3 independent experiments); *$p < 0.05$, **$p < 0.01$, ***$p < 0.001$, unpaired Student's t test.

increases genome-editing efficiency and is associated with a low rate of off-target effects (Liang et al., 2015). We sought to increase the efficiency of targeted t(11;22) translocations in hMSCs by simultaneously nucleofecting two in vitro-assembled RNP complexes targeting both breakpoint regions formed by a combination of a 3xNLS Cas9 nuclease (IDT) and in vitro transcribed sgRNA#1 or sgRNA#2. We first optimized the amount of RNPs by nucleofecting GFP-expressing HEK293 cells with increasing doses of GFP-targeting Cas9-sgRNA RNPs (0.5–4 μg). FACS analysis 72 hr post transfection showed that the percentage of GFP^+ HEK293 cells was optimal after nucleofection with 2 μg of GFP-targeting Cas9-sgRNA RNPs (Figure S5). We therefore compared the efficiency of Cas9 delivery with 2 μg of RNPs versus 2 μg of pLV-$U6^{\#1}H1^{\#2}$-C9G *all-in-one* CRISPR vector. FISH analysis 72 hr after nucleofection revealed that, compared with plasmid-based Cas9/sgRNA expression, translocation editing with the RNP approach was 9-fold more efficient in HEK293 cells (from 0.39% to 3.66%) and 12-fold more efficient in hMSCs (from 0.08% to 1.00%) (Figure 5C). The increased frequency of $t(11;22)^+$ cells when the RNPs were used was not associated with off-target effects at the predicted top off-target sites (http://crispr.mit.edu/ and https://benchling.com/) as determined by T7 endonuclease assay (Figure S3). Long-term culture assay coupled with FISH analysis of three independent $t(11;22)^+$ HEK293 cellular clones demonstrated stability of the derivative chromosomes (data not shown).

The outcome of the CRISPR/Cas9 optimization strategies undertaken in HEK293 cells and hMSCs prompted us to evaluate combinations of Cas9 RNP complexes with ssODNs or end-joining DNA processing factors for the generation of targeted t(11;22) translocation. hMSCs were nucleofected with RNPs alone or in combination with *translocation*-ssODNs or with the PARP1 or TREX end-joining factors. FISH analysis showed that the combination of RNPs and ssODNs increased the t(11;22) frequency in hMSCs by 2-fold (from 0.84% to 1.65%) (Figure 5D and Table S1). Interestingly, neither TREX2 nor PARP1 enzymes enhanced the efficiency of targeted t(11;22) translocation.

Generation of t(11;22) Translocation in Human iPSCs

In line with previous studies (Kovar et al., 2016), despite being possible to induce the t(11;22) in hMSCs over the short term, the fusion gene was not compatible with hMSC viability/homeostasis and the t(11;22)-edited hMSCs were progressively lost in culture (data not shown). Because Ewing sarcoma is composed by poorly differentiated cells

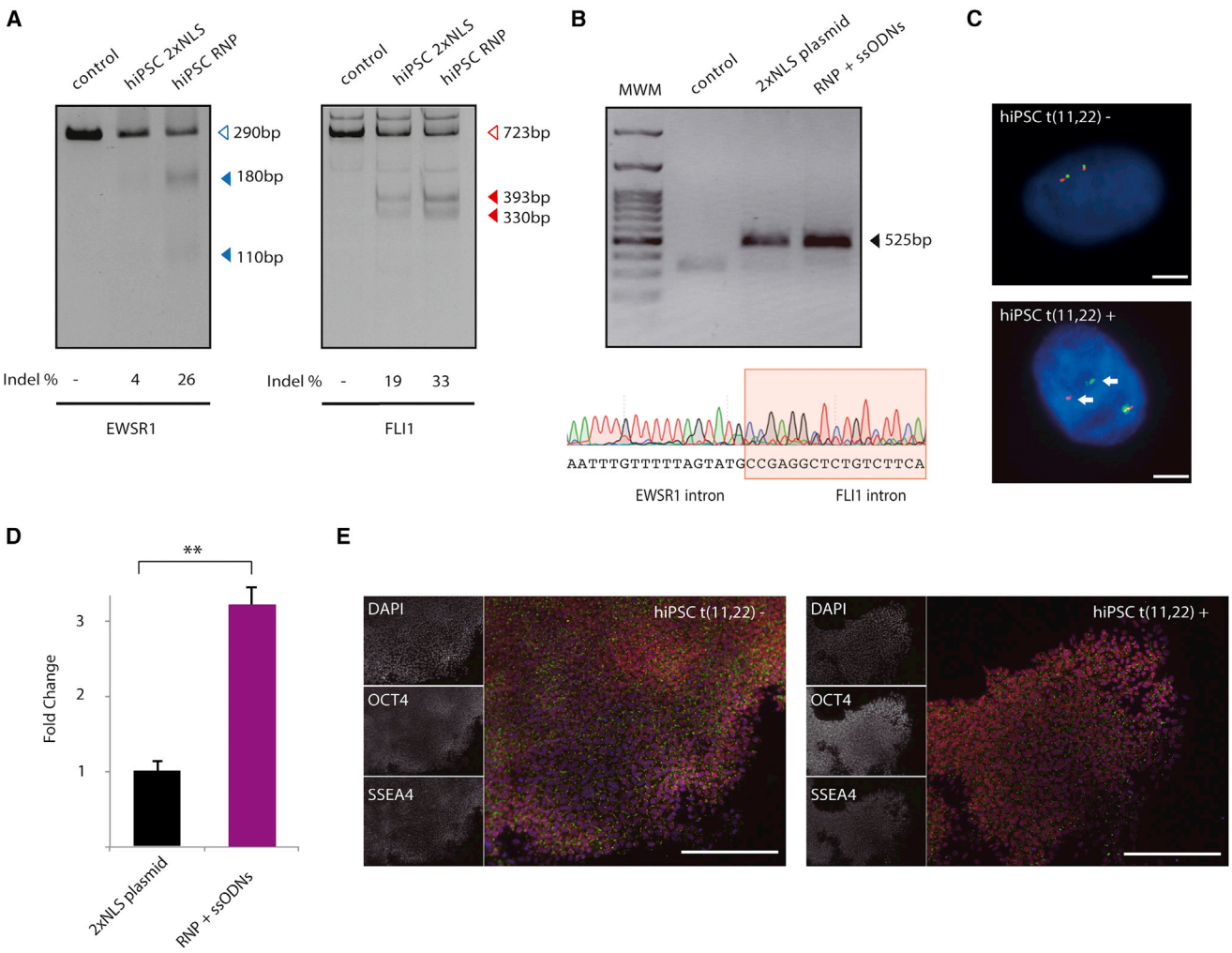

Figure 6. Induction of Targeted Chromosomal Translocation in hiPSCs

(A) Representative sgE1 and sgF2 on-target T7 endonuclease I assay in hiPSCs to determine the targeting activity of RNP complexes. Cells were transfected either with a non-targeting 3xNLS RNP complex (control), with 2xNLS plasmid, or with 3xNLS RNP complexes targeting both breakpoint regions. Open triangles depict the full-length PCR product and filled triangles the digestion products.

(B) Agarose gel electrophoresis of translocation-specific PCR products from pooled hiPSC samples. The Sanger sequencing chromatogram shows the breakpoint region in the *EWSR1-FLI1* fusion gene mapped at der(22).

(C) Representative FISH images obtained with a break-apart *EWSR1* probe showing hiPSCs positive and negative for t(11;22) generated with Cas9 RNP and ssODNs. Arrows indicate separated signals corresponding to the der(22) and der(11) breakpoint regions. Interphase nuclei are counterstained with DAPI. Scale bars, 10 μm.

(D) Fold-change variation in the number of engineered t(11;22) translocations determined by FISH in hiPSCs transfected with the 2xNLS-pLV-U6#1H1#2-C9G plasmid approach or with the RNP + ssODNs approach. Data are means ± SEM (n = 3 independent experiments); **p < 0.01, unpaired Student's t test.

(E) Immunostaining of t(11;22) positive and negative hiPSC colonies for the pluripotency markers OCT4 and SSEA4. Scale bars, 200 μm.

of unknown origin (Kovar et al., 2016), we next sought to generate the t(11;22) translocation in human iPSCs. These difficult-to-target cells are an invaluable biological tool for disease modeling and biomedical research (Sancho-Martinez et al., 2016). We first checked the on-target cleavage of hiPSCs edited with 2xNLS Cas9 plasmid or with 3xNLS RNP complexes targeting the *EWSR1* and *FLI1* loci. This assay revealed higher rates of genomic disruption when RNPs are used (4% versus 26% and 19% versus 33%, respectively) (Figure 6A). A single-cell suspension of hiPSCs was nucleofected with a combination of Cas9 RNPs and *translocation*-ssODNs, the most efficient approach optimized in hMSCs, with a 99.5% transfection efficiency as measured by a Cy3 oligonucleotide (Figure S4C). Junction PCR and

Sanger sequencing 72 hr after nucleofection revealed the generation of the t(11;22) translocation in the hiPSC population (Figure 6B), a result confirmed by FISH analysis (Figure 6C). FISH analysis confirmed that co-nucleofection with RNP complexes and ssODNs increased translocation frequency by 3.2-fold (from 0.42% to 1.39%) compared with the 2xNLS approach (Figure 6D). Importantly, hiPSCs were subcloned and a t(11;22)$^{+}$ hiPSC clone was expanded for 8 weeks, revealing maintenance of the translocation (Figure S6), with no differences in cell/colony morphology, expression of the pluripotency markers OCT4 and SSEA-4, and growth rate (Figure 6E).

DISCUSSION

We have developed an optimized and streamlined method for efficient engineering of targeted chromosomal translocations in human MSCs and iPSCs. We first generated an all-in-one plasmid system to co-express two sgRNAs, the *Streptococcus pyogenes* Cas9 flanked by two NLSs and an EGFP reporter. This all-in-one plasmid system enhanced successful delivery of CRISPR components and allowed FACS selection of transfected cells, thus maximizing the frequency of cells targeted by CRISPR/Cas9 and improving nuclear protein uptake and its subsequent genome engineering activity without observed off-target effects. Unlike other strategies, our expression vector provides simultaneous expression of CRISPR elements and an improved nuclear uptake of the Cas9 protein. Compared with the all-in-one 1xNLS approach, the 2xNLS version yielded 3.6-fold and 7.1-fold higher translocation rates for the Ewing sarcoma t(11;22) translocation in HEK293 cells and human MSCs, suggesting that this strategy is a robust tool for targeted translocations. The different genome-editing efficiencies in HEK293 cells and hMSCs clearly reflect differences in biology and genetic background between unstable cell lines and human stem cells.

To further increase targeted translocation with the CRISPR/Cas9 system, we devised two improvements. The first approach involves co-nucleofection of two *translocation*-ssODNs for efficient guidance of the broken chromosomes. Donor ssODNs composed of homology arms flanking the genomic modification site have been used to increase targeting efficiencies in human stem cells (Chen et al., 2011; Kim and Kim, 2014; Yang et al., 2013), and recent reports exploited ssODNs to improve CRISPR deletion approaches (Yoshimi et al., 2016). We therefore hypothesized that donor ssODN templates containing homology arms flanking the junction region of a translocation-derived chromosome breakpoint would guide the rejoining of the derivative chromosome, thus facilitating translocation. The concurrent use of two 150-nt-long ssODN donor translocation templates complementary to each derivative chromosome yielded an 11-fold increase in hMSC translocation efficiency. This effect was crucially influenced by ssODN donor length. Shorter ssODNs might be too weak to guide HDR, whereas longer ssODNs might be less accessible to the genome repair machinery, perhaps due to secondary structure constraints. Further details of this mechanism will await future studies on the dynamics of chromosomal translocations and the role of HRD.

The second approach is based on the co-expression of end-joining DNA-processing factors. Although the breakage mechanisms of chromosomal translocations are not completely understood, the rejoining mechanism is usually via NHEJ, the predominant DSB repair pathway when no DNA template is available. NHEJ is mediated by two subpathways, classical (cNHEJ), initiated by the Ku complex, and alternative (altNHEJ), initiated by poly ADP-ribose polymerase 1 (PARP1); each subpathway has distinct mutational consequences (Audebert et al., 2004; Castaño et al., 2016; Howard et al., 2015). The cNHEJ repair pathway suppresses the formation of chromosome translocations but sometimes induces sequence alterations at the junction regions. The altNHEJ pathway operates when the cNHEJ pathway is inactivated, and is associated with a higher probability of chromosome translocations and the generation of larger sequence alterations at junction breakpoints (Iliakis et al., 2015). Recent reports suggest that the altNHEJ pathway typically recognizes sequence microhomologies and is more translocation prone (Audebert et al., 2006; Certo et al., 2012; Wray et al., 2013), and this pathway has been linked to chromosome translocations in mouse cells, *Drosophila*, and yeast (McVey et al., 2004; Simsek and Jasin, 2010). Thus, altNHEJ seems to be responsible for the elimination from the genome of highly cytotoxic DNA DSBs, but at the cost of increasing the generation of translocations. However, it is unclear how one DSB-processing pathway is selected over the other. DNA end-processing factors involved in the cNHEJ and altNHEJ repair mechanisms have been used to improve the efficiency of gene disruption genome engineering in combination with ZFN and TALENs (Certo et al., 2012). Increases in mutagenesis rate of up to 25-fold have been reported upon coupling of ZFN endonucleases to DNA end-processing enzymes to drive targeted gene disruption (Certo et al., 2012). We assessed whether co-expressing the CRISPR/Cas9 system with a panel of DNA end-processing factors could increase the targeted translocation rate. TREX2 and PARP1 produced a 2-fold increase in hMSC translocation rates, showing that coupling them with the CRISPR/Cas9 system provides an alternative route to increasing translocation rates in human stem cells.

Delivery of Cas9 protein in an RNP complex with the sgRNA avoids the need for in vivo transcription and translation. Moreover, this approach yields high expression shortly after nucleofection, followed by rapid degradation, thereby facilitating efficient gene editing while minimizing off-target rates. The good performance of the RNP approach in genome-engineering experiments (Liang et al., 2015) may be related to three factors: (1) the possibility to better control the complexing process in vitro, (2) the protection of the Cas9-complexed guide RNA from cellular degradation, and (3) the avoidance of DNA-based cellular toxicity. We found that the combined use of two RNP complexes greatly improves the efficiency of generating targeted translocations in hMSCs, yielding a 12-fold higher rate than the all-in-one plasmid approach. Translocation rates were further improved by co-nucleofecting RNPs and *translocation*-ssODNs, demonstrating a synergistic effect between these approaches. Surprisingly, translocation rate was not increased by the combined use of RNPs and DNA end-processing enzymes. This might be due to Cas9 RNP degradation preceding expression of the vector-encoded DNA end-processing factors.

Although a combination of 3xNLS-RNPs and ssODNs efficiently induced the t(11;22) translocation in hMSCs, this particular translocation was unstable in this cell type, and cells harboring this rearrangement were eventually lost in culture. This finding is in agreement with recent studies of Ewing sarcoma suggesting that MSCs might not represent the target cell-for-transformation in Ewing sarcoma (Kovar et al., 2016; Minas et al., 2016; Renouf et al., 2014; Rodriguez et al., 2011). We therefore attempted to induce the t(11;22) translocation in a less differentiated cell type. We chose hiPSCs because their pluripotent/developmentally early nature as iPSC derivatives constitutes a valid cellular system for disease modeling, including cancer development (Bueno et al., 2011; Menendez et al., 2006; Muñoz-López et al., 2016). Co-nucleofection with RNPs and *translocation*-ssODNs was able to induce targeted t(11;22) translocations in hiPSCs while maintaining the pluripotent phenotype. These t(11;22)-harboring iPSCs would therefore represent a major step forward in modeling the developmental impact of cancer-associated chromosomal translocations. It allows the investigation of the mechanistic basis and clonal properties of human Ewing sarcoma and would help us to understand the relative contributions of genetic and epigenetic developmental abnormalities to Ewing sarcoma, thus assisting in the integrated design of targeted therapies.

The coupled RNP-ssODN CRISPR/Cas9 approach presented here supports efficient targeted translocation induction, and enables rapid and efficient targeted translocation in hMSCs and hiPSCs. This approach is applicable to human stem cells, facilitating the combination of the power of human stem cell technology with the CRISPR/Cas9 genome-engineering system for cancer disease modeling. Translocations induced with the CRISPR/Cas9 system avoid potential complications associated with overexpression of fusion genes and transgene variegation while at the same time recreating the translocated genome architecture, including the spatial organization and regulatory elements. Moreover, the use of the CRISPR/Cas9 approach to reproduce chromosomal translocations allows the generation of isogenic cell lines, facilitating study of the effects of individual rearrangements.

The methodological approaches presented here for efficient generation of chromosomal translocations in hMSCs and hiPSCs have potential applications in a diverse range of cell types, and can be used to generate diverse genome rearrangements, including large deletions or inversions. RNPs can also be engineered and used for other gene-editing approaches. This strategy will likely facilitate cancer modeling with human stem cells and precise genome engineering for cell therapy approaches and drug-screening strategies, accelerating bench-to-bedside translation into preclinical studies.

EXPERIMENTAL PROCEDURES

Cell Culture

The HEK293 cell line (CRL-1573, ATCC) was maintained under standard conditions in DMEM (Lonza) supplemented with 10% fetal bovine serum (FBS), 1% GlutaMAX, and 10 mg/mL penicillin-streptomycin (all from Life Technologies). Umbilical cord blood-derived hMSCs (PCS-500-010, ATCC) were cultured in MesenPRO RS medium supplemented with MesenPRO growth supplement (Life Technologies). Cells were cultured at 37°C in a humidified atmosphere with 5% CO_2 and 20% O_2. hiPSCs were maintained under feeder-free conditions on Matrigel (BD Biosciences) in mTeSR1 medium (STEMCELL Technologies). Cultures were dispersed to single-cell suspensions using Accutase (STEMCELL). Cell survival before nucleofection was promoted with the Rho-associated kinase (ROCK) inhibitor Y-27632 (10 μM; Selleckchem). hiPSCs were generated in P.M.'s laboratory from human $CD34^+$ cells from peripheral blood mononuclear cells using OKSM polycistronic SeV vectors (Muñoz-López et al., 2016). hiPSC research was approved by the ISCIII Steering Committee on pluripotent stem cell research.

Construction of Double-Guide Cas9-Encoding Plasmids, End-Joining DNA-Processing Factor Expression Plasmids, and ssODNs

The parental pLV-sgRNA-Cas9 vector has been described elsewhere (Torres et al., 2014b). The CMV promoter was PCR-amplified from pcDNA3.1 (Life Technologies), and the H1 promoter was assembled from gBlocks gene fragments (IDT). The CMV and H1 promoters were cloned into pLV-sgRNA-Cas9. Two gBlocks gene fragments were synthesized to clone sgRNA#1 and sgRNA#2 in the

backbone vector, thus creating the pLV-U6$^{\#1}$H1$^{\#2}$-C9 construct. The 2A-eGFP fragment was obtained from a construct generated in-house (pKAS; Torres et al., 2014a), and a linker was used to generate the final pLV-U6$^{\#1}$H1$^{\#2}$-C9G vector (Figure 1A).

The altNHEJ factor expression vectors pExodus.CMV.Artemis and pExodus.CMV.Trex2 (Certo et al., 2012) were obtained from Addgene. pCMV6-PARP1, pCMV6-MRE11, and pCMV6-FEN1 were obtained from OriGene Technologies. ssODNs were purchased from IDT as 4-nmol ultramer DNA oligos. Nucleoplasmin NLS (Torres and Ramirez, 2009) was cloned at the 5′ end of the Cas9 sequence, creating the pLV-U6$^{\#1}$H1$^{\#2}$-C9G-2xNLS plasmid.

Cas9 Ribonucleoproteins

Recombinant Cas9 protein was obtained from IDT and sgRNAs were in vitro transcribed through runoff reactions by T7 RNA polymerase using the HiScribe T7 high-yield RNA synthesis kit (NEB). Transcribed sgRNAs were purified with a column purification kit (RNeasy mini kit, Qiagen), quantified, and quality checked by denaturing RNA gel electrophoresis. For generation of RNP complexes, Cas9 protein (1–8 μg) was premixed with in vitro transcribed sgRNA (0.5–8 μg) for 10 min at room temperature.

Transfection and Electroporation

Cells were transfected as previously described (Torres et al., 2014a). For electroporation, the Neon Transfection System was used (Thermo Fisher Scientific). Confluent hMSCs, hiPSCs, and HEK293 cells were trypsinized, resuspended in R solution, and electroporated using the following conditions. For hMSCs, 10-μL tips were used to electroporate 1×10^5 cells with a single 40-ms pulse of 990 V. For HEK293 cells, 4×10^5 cells were electroporated with 10-μL tips using three 10-ms pulses of 1,245 V. Finally, hiPSCs were electroporated with 10-μL tips using 2×10^5 cells with three 5-ms pulses of 1,400 V. After electroporation, cells were seeded in a 24-well plate containing prewarmed medium. When required, cells were sorted 72 hr post transfection. For co-transfection experiments, 200 pmol of ssODN (IDT) or end-processing plasmids were included.

Immunofluorescence

Immunofluorescence was carried out as previously described, with modifications (Torres and Ramirez, 2009).

Image Acquisition and Nucleus/Cytoplasm Ratio

Images were acquired on a TCS-SP5 confocal microscope from Leica microsystems using a 20× HCX PL APO dry objective (numerical aperture 0.7). Nucleus and cytoplasmic signal for each cell was segmented and quantified using a customized script in Definiens Developer XD software v2.5 (Definiens). The nucleus/cytoplasm value represents the ratio between the average nuclear fluorescence intensity of the cell population and the average cytoplasmic fluorescence intensity between their own nuclei.

Flow Cytometry and Cell Sorting

Seventy-two hours after transfection or electroporation, cells were trypsinized, washed twice with Dulbecco's PBS, counted, and resuspended in an appropriate volume of sorting buffer (PBS containing 1% FBS and antibiotics). Prior to cell sorting, samples were filtered through a 70-μm filter to remove any cell clumps. Cell sorting was carried out in a Synergy 2L instrument (Sony Biotechnology). Flow-cytometry acquisition and analysis was performed in a BD LSR Fortessa Analyzer (BD Biosciences). A gating strategy was performed to remove clumps or doublets from the dataset (pulse geometry gating), to remove dead cells (DAPI viability gating), and to remove debris and other events of non-interest while preserving cells based on size and/or complexity (forward- and side-scatter gating).

Genomic DNA Extraction and PCR Analysis

Genomic DNA was extracted using standard procedures. Primers used are listed in Table S1.

Fluorescence In Situ Hybridization

For FISH analysis, HEK293, hMSC, and hiPSC cultures were first arrested in metaphase by incubation for 2–4 hr at 37°C with KaryoMAX Colcemid (0.1 μg/mL) (Thermo Fisher) and then harvested after treatment with a hypotonic salt solution. A break-apart EWSR1 FISH probe (Cytocell) was used to detect the t(11;22) chromosomal translocation. Chromosome spreads were left overnight at room temperature. Slides were dehydrated through a series of ethanol washes, denatured in the presence of the EWSR1 probe on a plate at 75°C for 1 min, and hybridized overnight at 37°C. After post-hybridization washes, the chromosomes were counterstained with DAPI in Vectashield Mounting Medium (Vector Laboratories). FISH evaluation was performed by visual evaluation of between 200 and 1,000 cells. Cell images were captured using a cooled charge-coupled device camera and analyzed with the Chromofluor image analysis system (CytoVision, Leica Biosystems).

Detection of Indels by T7 Endonuclease I Assay

Seventy-two hours after nucleofection, genomic DNA was isolated with a DNA purification kit (Qiagen). The negative control sample (empty) is the DNA extracted from cells transfected with the *all-in-one* plasmid expressing a truncated sgRNA that lacks the base-pairing region but which contains the Cas9-binding hairpin, allowing the sgRNA to form a complex with Cas9. PCR reactions were carried out with Q5 high-fidelity DNA polymerase (NEB). Each product was confirmed by gel electrophoresis and further purified on a Qiaquick Spin Column (Qiagen). A total of 350 ng of each PCR product was reannealed in a final volume of 20 μL of NEB Buffer 2, in order to form heteroduplexes. Products were then processed with the T7 endonuclease I (NEB) and separated on an 8% polyacrylamide Tris/borate/EDTA (TBE) gel. Gels were stained with SYBR Gold (Thermo Fisher) for 20 min and washed with 1× TBE for 10 min. Cas9-mediated cleavage efficiency (indel percentage) is calculated on the basis of the fraction of cleaved DNA, as determined by integrated intensity of gel bands. Images were acquired with the Gel Doc imaging system (Bio-Rad), and relative band intensities were quantified with ImageJ. NHEJ frequency was quantified using the formula $100 \times (1 - (1 - a/(a + b))1/2)$, where a is the band intensity of the cleavage products and b is the band intensity of the uncleaved PCR product.

Lentivirus Generation, Titration, and Transduction

Viruses were produced by transient plasmid transfection into HEK293 cells using the calcium phosphate method (Torres et al., 2011).

Statistical Analysis

Data from three or more independent experiments were analyzed by two-tailed unpaired t test. In the figures, significance is denoted by *p < 0.05, **p < 0.01, ***p < 0.001, and ****p < 0.0001.

SUPPLEMENTAL INFORMATION

Supplemental Information includes Supplemental Experimental Procedures, six figures, and two tables and can be found with this article online at http://dx.doi.org/10.1016/j.stemcr.2017.04.014.

AUTHOR CONTRIBUTIONS

R.T.-R. and S.R.-P. designed and performed experiments, analyzed the data, and wrote the manuscript; M.M.-L., M.C.M., and A.G. assisted in the experiments and collected data; P.M. wrote the manuscript; J.C.C. and J.C.R. analyzed the data and commented on the manuscript; C.B. and J.C. commented on the manuscript.

ACKNOWLEDGMENTS

This work was supported by funds from the Spanish National Research and Development Plan, Instituto de Salud Carlos III, and FEDER (PI14/01884 to S.R.-P. and PI12/00425 to J.C.C.). R.T.-R. was supported by an international fellowship from Lady Tata Memorial Trust during 2016–2017.

Received: August 30, 2016
Revised: April 12, 2017
Accepted: April 12, 2017
Published: May 9, 2017

REFERENCES

Audebert, M., Salles, B., and Calsou, P. (2004). Involvement of poly(ADP-ribose) polymerase-1 and XRCC1/DNA ligase III in an alternative route for DNA double-strand breaks rejoining. J. Biol. Chem. *279*, 55117–55126.

Audebert, M., Salles, B., Weinfeld, M., and Calsou, P. (2006). Involvement of polynucleotide kinase in a poly (ADP-ribose) polymerase-1-dependent DNA double-strand breaks rejoining pathway. J. Mol. Biol. *356*, 257–265.

Blasco, R.B., Karaca, E., Ambrogio, C., Cheong, T.-C., Karayol, E., Minero, V.G., Voena, C., and Chiarle, R. (2014). Simple and rapid in vivo generation of chromosomal rearrangements using CRISPR/Cas9 technology. Cell Rep. *9*, 1219–1227.

Brunet, E., Simsek, D., Tomishima, M., DeKelver, R., Choi, V.M., Gregory, P., Urnov, F., Weinstock, D.M., and Jasin, M. (2009). Chromosomal translocations induced at specified loci in human stem cells. Proc. Natl. Acad. Sci. USA *106*, 10620–10625.

Bueno, C., Montes, R., Catalina, P., Rodríguez, R., and Menendez, P. (2011). Insights into the cellular origin and etiology of the infant pro-B acute lymphoblastic leukemia with MLL-AF4 rearrangement. Leukemia *25*, 400–410.

Castaño, J., Herrero, A.B., Bursen, A., González, F., Marschalek, R., Gutiérrez, N.C., and Menendez, P. (2016). Expression of MLL-AF4 or AF4-MLL fusions does not impact the efficiency of DNA damage repair. Oncotarget *7*, 30440–30452.

Certo, M.T., Gwiazda, K.S., Kuhar, R., Sather, B., Curinga, G., Mandt, T., Brault, M., Lambert, A.R., Baxter, S.K., Jacoby, K., et al. (2012). Coupling endonucleases with DNA end-processing enzymes to drive gene disruption. Nat. Methods *9*, 973–975.

Chen, J.-M., Cooper, D.N., Férec, C., Kehrer-Sawatzki, H., and Patrinos, G.P. (2010). Genomic rearrangements in inherited disease and cancer. Semin. Cancer Biol. *20*, 222–233.

Chen, F., Pruett-Miller, S.M., Huang, Y., Gjoka, M., Duda, K., Taunton, J., Collingwood, T.N., Frodin, M., and Davis, G.D. (2011). High-frequency genome editing using ssDNA oligonucleotides with zinc-finger nucleases. Nat. Methods *8*, 753–755.

Chen, Z., Jaafar, L., Agyekum, D.G., Xiao, H., Wade, M.F., Kumaran, R.I., Spector, D.L., Bao, G., Porteus, M.H., Dynan, W.S., and Meiler, S.E. (2013). Receptor-mediated delivery of engineered nucleases for genome modification. Nucleic Acids Res. *41*, e182.

Cong, L., Ran, F.A., Cox, D., Lin, S., Barretto, R., Habib, N., Hsu, P.D., Wu, X., Jiang, W., Marraffini, L.A., and Zhang, F. (2013). Multiplex genome engineering using CRISPR/Cas systems. Science *339*, 819–823.

Delattre, O., Zucman, J., Melot, T., Garau, X.S., Zucker, J.M., Lenoir, G.M., Ambros, P.F., Sheer, D., Turc-Carel, C., and Triche, T.J. (1994). The Ewing family of tumors–a subgroup of small-round-cell tumors defined by specific chimeric transcripts. N. Engl. J. Med. *331*, 294–299.

Forster, A., Pannell, R., Drynan, L., Cano, F., Chan, N., Codrington, R., Daser, A., Lobato, N., Metzler, M., Nam, C.-H., et al. (2005). Chromosomal translocation engineering to recapitulate primary events of human cancer. Cold Spring Harb. Symp. Quant. Biol. *70*, 275–282.

Gaj, T., Guo, J., Kato, Y., Sirk, S.J., and Barbas, C.F. (2012). Targeted gene knockout by direct delivery of zinc-finger nuclease proteins. Nat. Methods *9*, 805–807.

Guryanova, O.A., and Levine, R.L. (2013). Advances in the development of animal models of myeloid leukemias. Semin. Hematol. *50*, 145–155.

Howard, S.M., Yanez, D.A., and Stark, J.M. (2015). DNA damage response factors from diverse pathways, including DNA crosslink repair, mediate alternative end joining. PLoS Genet. *11*, e1004943.

Iliakis, G., Murmann, T., and Soni, A. (2015). Alternative end-joining repair pathways are the ultimate backup for abrogated classical non-homologous end-joining and homologous recombination repair: implications for the formation of chromosome translocations. Mutat. Res. Genet. Toxicol. Environ. Mutagen *793*, 166–175.

Jinek, M., Chylinski, K., Fonfara, I., Hauer, M., Doudna, J.A., and Charpentier, E. (2012). A programmable dual-RNA-guided DNA endonuclease in adaptive bacterial immunity. Science *337*, 816–821.

Kim, H., and Kim, J.-S. (2014). A guide to genome engineering with programmable nucleases. Nat. Rev. Genet. *15*, 321–334.

Kim, S., Kim, D., Cho, S.W., Kim, J., and Kim, J.-S. (2014). Highly efficient RNA-guided genome editing in human cells via delivery of purified Cas9 ribonucleoproteins. Genome Res. *24*, 1012–1019.

Kovar, H., Amatruda, J., Brunet, E., Burdach, S., Cidre-Aranaz, F., and de Alva, E. (2016). The second European interdisciplinary Ewing sarcoma research summit—a joint effort to deconstructing the multiple layers of a complex disease. Oncotarget *7*, 8613–8624.

Li, K., Wang, G., Andersen, T., Zhou, P., and Pu, W.T. (2014). Optimization of genome engineering approaches with the CRISPR/Cas9 system. PLoS One *9*, e105779.

Liang, X., Potter, J., Kumar, S., Zou, Y., Quintanilla, R., Sridharan, M., Carte, J., Chen, W., Roark, N., Ranganathan, S., et al. (2015). Rapid and highly efficient mammalian cell engineering via Cas9 protein transfection. J. Biotechnol. *208*, 44–53.

Liu, J., Gaj, T., Wallen, M.C., and Barbas, C.F. (2015). Improved cell-penetrating zinc-finger nuclease proteins for precision genome engineering. Mol. Ther. Nucleic Acids *4*, e232.

Maddalo, D., Manchado, E., Concepcion, C.P., Bonetti, C., Vidigal, J.A., Han, Y.-C., Ogrodowski, P., Crippa, A., Rekhtman, N., de Stanchina, E., et al. (2014). In vivo engineering of oncogenic chromosomal rearrangements with the CRISPR/Cas9 system. Nature *516*, 423–427.

Mali, P., Yang, L., Esvelt, K.M., Aach, J., Guell, M., DiCarlo, J.E., Norville, J.E., and Church, G.M. (2013). RNA-guided human genome engineering via Cas9. Science *339*, 823–826.

McVey, M., Radut, D., and Sekelsky, J.J. (2004). End-joining repair of double-strand breaks in Drosophila melanogaster is largely DNA ligase IV independent. Genetics *168*, 2067–2076.

Menendez, P., Bueno, C., and Wang, L. (2006). Human embryonic stem cells: a journey beyond cell replacement therapies. Cytotherapy *8*, 530–541.

Minas, T.Z., Surdez, D., Javaheri, T., Tanaka, M., Howarth, M., Kang, H.-J., Han, J., Han, Z.-Y., Sax, B., Kream, B.E., et al. (2016). Combined experience of six independent laboratories attempting to create an Ewing sarcoma mouse model. Oncotarget *9*, 422–434.

Muñoz-López, A., Romero-Moya, D., Prieto, C., Ramos-Mejía, V., Agraz-Doblas, A., Varela, I., Buschbeck, M., Palau, A., Carvajal-Vergara, X., Giorgetti, A., et al. (2016). Development refractoriness of MLL-rearranged human B cell acute leukemias to reprogramming into pluripotency. Stem Cell Rep. *7*, 602–618.

Piganeau, M., Ghezraoui, H., De Cian, A., Guittat, L., Tomishima, M., Perrouault, L., René, O., Katibah, G.E., Zhang, L., Holmes, M.C., et al. (2013). Cancer translocations in human cells induced by zinc finger and TALE nucleases. Genome Res. *23*, 1182–1193.

Ramakrishna, S., Kwaku Dad, A.-B., Beloor, J., Gopalappa, R., Lee, S.-K., and Kim, H. (2014). Gene disruption by cell-penetrating peptide-mediated delivery of Cas9 protein and guide RNA. Genome Res. *24*, 1020–1027.

Renouf, B., Piganeau, M., Ghezraoui, H., Jasin, M., and Brunet, E. (2014). Creating cancer translocations in human cells using Cas9 DSBs and nCas9 paired nicks. Meth. Enzymol. *546*, 251–271.

Rodriguez, R., Rubio, R., and Menendez, P. (2011). Modeling sarcomagenesis using multipotent mesenchymal stem cells. Cell Res. *22*, 62–77.

Rodriguez-Perales, S., Torres-Ruiz, R., Suela, J., Acquadro, F., Martin, M.C., Yebra, E., Ramirez, J.C., Alvarez, S., and Cigudosa, J.C. (2015). Truncated RUNX1 protein generated by a novel t(1;21)(p32;q22) chromosomal translocation impairs the proliferation and differentiation of human hematopoietic progenitors. Oncogene *35*, 125–134.

Sancho-Martinez, I., Nivet, E., Xia, Y., Hishida, T., Aguirre, A., Ocampo, A., Ma, L., Morey, R., Krause, M.N., Zembrzycki, A., et al. (2016). Establishment of human iPSC-based models for the study and targeting of glioma initiating cells. Nat. Commun. *7*, 10743.

Simsek, D., and Jasin, M. (2010). Alternative end-joining is suppressed by the canonical NHEJ component Xrcc4-ligase IV during chromosomal translocation formation. Nat. Struct. Mol. Biol. *17*, 410–416.

Torres, R., and Ramirez, J.C. (2009). A chemokine targets the nucleus: Cxcl12-gamma isoform localizes to the nucleolus in adult mouse heart. PLoS One *4*, e7570.

Torres, R., García, A., Payá, M., and Ramirez, J.C. (2011). Non-integrative lentivirus drives high-frequency cre-mediated cassette exchange in human cells. PLoS One *6*, e19794.

Torres, R., Garcia, A., Jimenez, M., Rodriguez, S., and Ramirez, J.C. (2014a). An integration-defective lentivirus-based resource for site-specific targeting of an edited safe-harbour locus in the human genome. Gene Ther. *21*, 343–352.

Torres, R., Martin, M.C., Garcia, A., Cigudosa, J.C., Ramirez, J.C., and Rodriguez-Perales, S. (2014b). Engineering human tumour-associated chromosomal translocations with the RNA-guided CRISPR-Cas9 system. Nat. Commun. *5*, 3964.

Van Deursen, J., Fornerod, M., Van Rees, B., and Grosveld, G. (1995). Cre-mediated site-specific translocation between nonhomologous mouse chromosomes. Proc. Natl. Acad. Sci. USA *92*, 7376–7380.

Wray, J., Williamson, E.A., Singh, S.B., Wu, Y., Cogle, C.R., Weinstock, D.M., Zhang, Y., Lee, S.-H., Zhou, D., Shao, L., et al. (2013). PARP1 is required for chromosomal translocations. Blood *121*, 4359–4365.

Yang, L., Guell, M., Byrne, S., Yang, J.L., De Los Angeles, A., Mali, P., Aach, J., Kim-Kiselak, C., Briggs, A.W., Rios, X., et al. (2013). Optimization of scarless human stem cell genome editing. Nucleic Acids Res. *41*, 9049–9061.

Yoshimi, K., Kunihiro, Y., Kaneko, T., Nagahora, H., Voigt, B., and Mashimo, T. (2016). ssODN-mediated knock-in with CRISPR-Cas for large genomic regions in zygotes. Nat. Commun. *7*, 10431.

Stem Cell Reports, Volume *8*

Supplemental Information

Efficient Recreation of t(11;22) *EWSR1-FLI1*$^{+}$ in Human Stem Cells Using CRISPR/Cas9

Raul Torres-Ruiz, Marta Martinez-Lage, Maria C. Martin, Aida Garcia, Clara Bueno, Julio Castaño, Juan C. Ramirez, Pablo Menendez, Juan C. Cigudosa, and Sandra Rodriguez-Perales

A

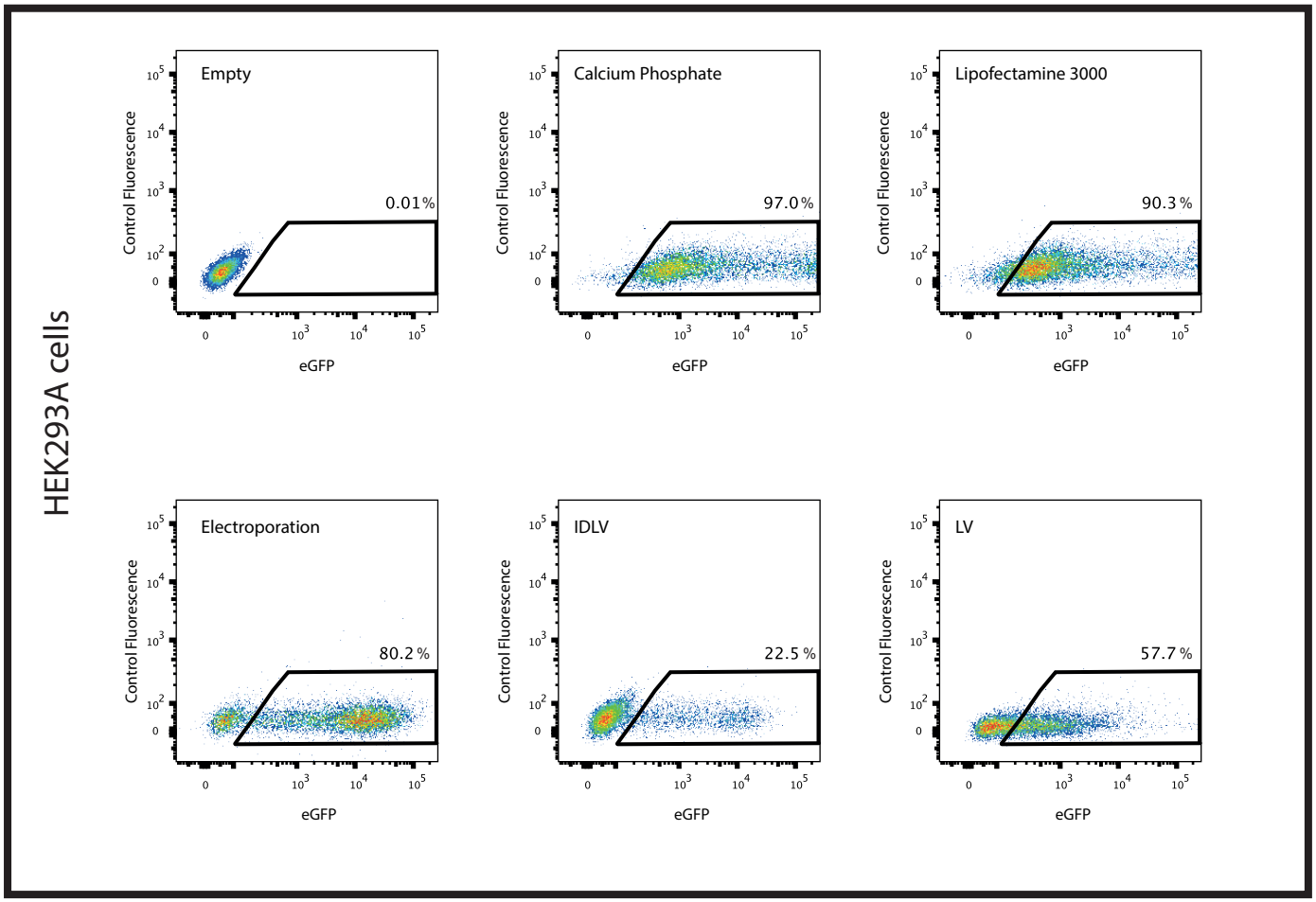
HEK293A cells
Empty
0.01%
Calcium Phosphate
97.0%
Lipofectamine 3000
90.3%
Electroporation
80.2%
IDLV
22.5%
LV
57.7%
Control Fluorescence
eGFP

B

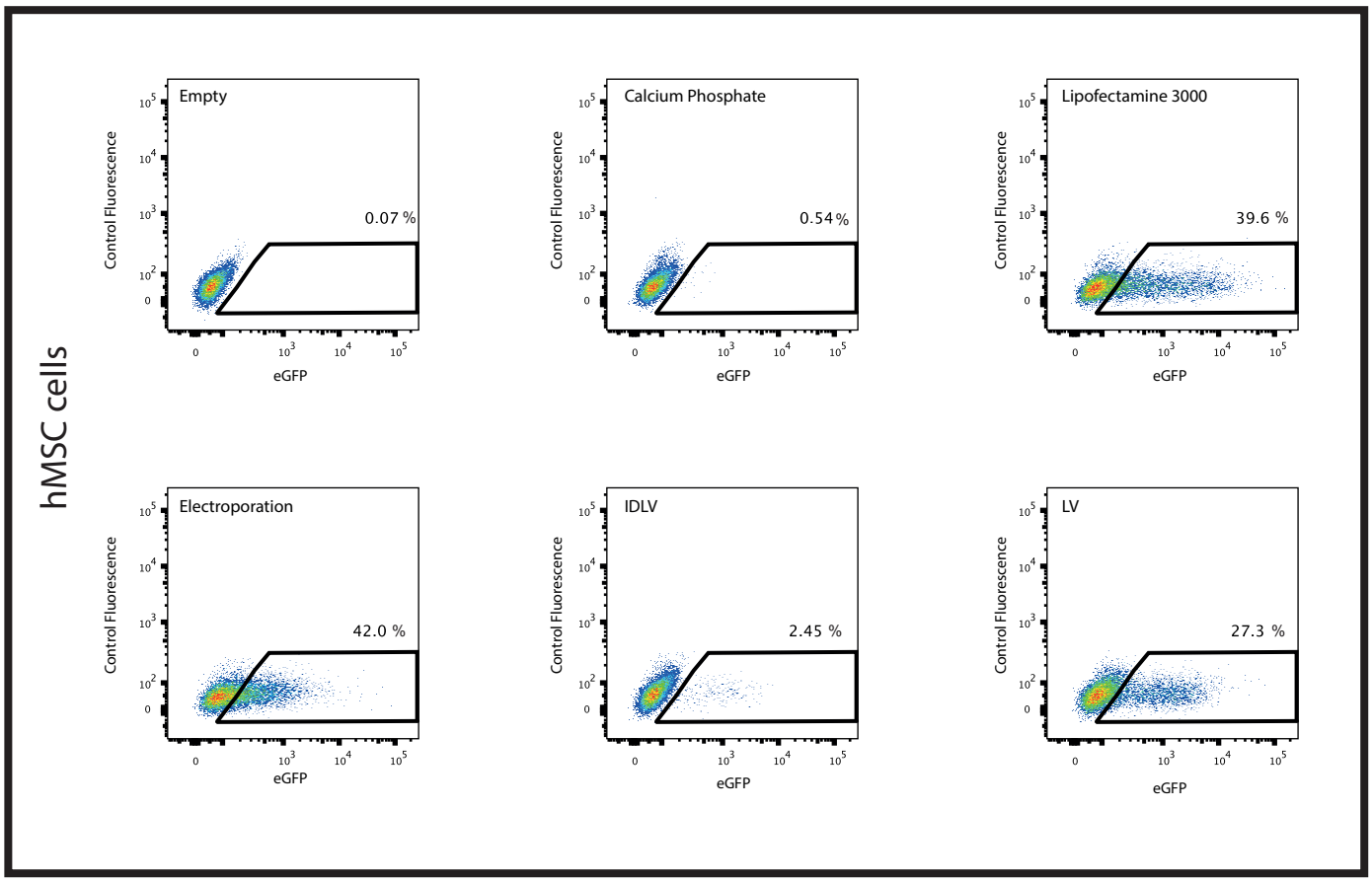
hMSC cells
Empty
0.07%
Calcium Phosphate
0.54%
Lipofectamine 3000
39.6 %
Electroporation
42.0 %
IDLV
2.45 %
LV
27.3 %
Control Fluorescence
eGFP

A

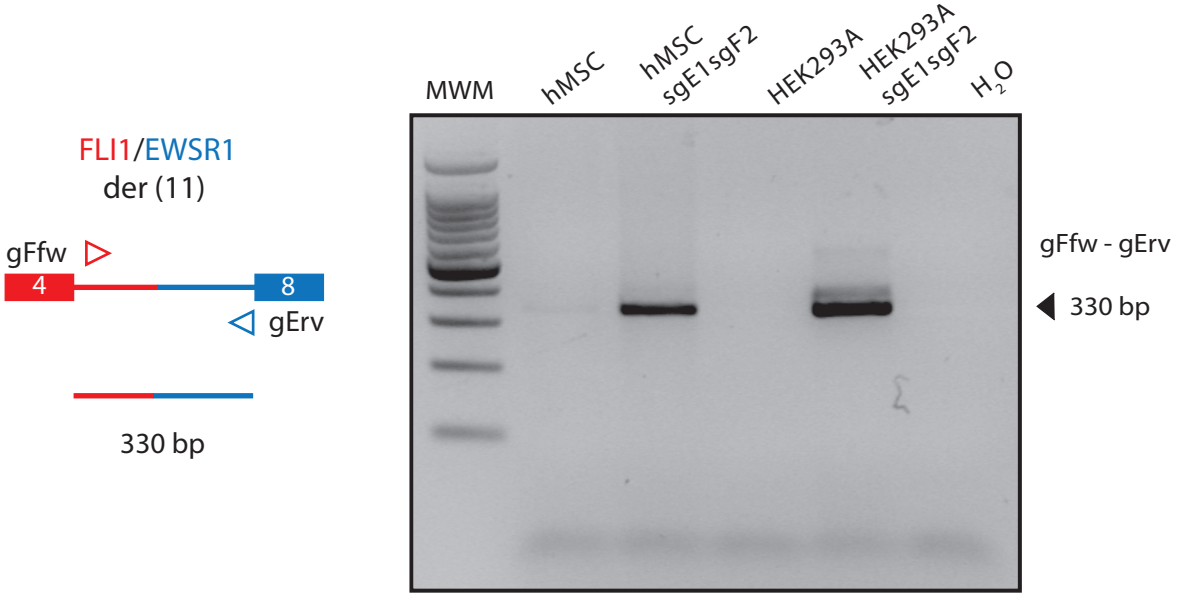
FLI1/EWSR1
der (11)
gFfw
4
8
gErv
330 bp
MWM
hMSC
hMSC sgE1sgF2
HEK293A
HEK293A sgE1sgF2
H2O
gFfw - gErv
330 bp

B

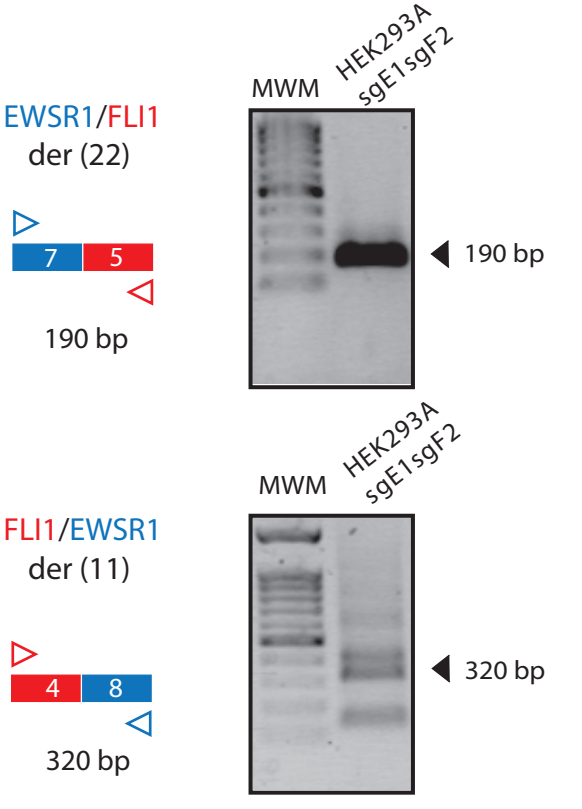
EWSR1/FLI1
der (22)
7
5
190 bp
MWM
HEK293A sgE1sgF2
190 bp
FLI1/EWSR1
der (11)
4
8
320 bp
MWM
HEK293A sgE1sgF2
320 bp

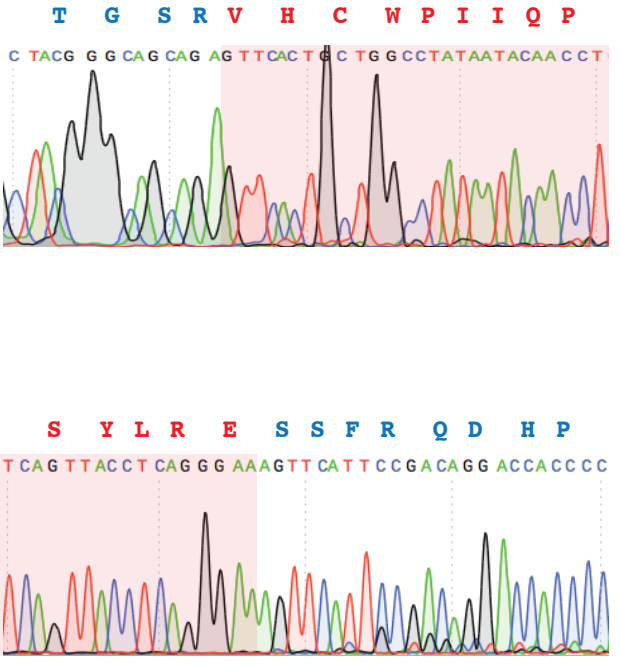
T G S R V H C W P I I Q P
C TACG G G CAG CAG AG TTCAC T G C TG G CCTATAATACAACCT
S Y L R E S S F R Q D H P
T CAG TTACCT CAGG G AAAGTT CATT CCGACAGG ACCACCCC

C

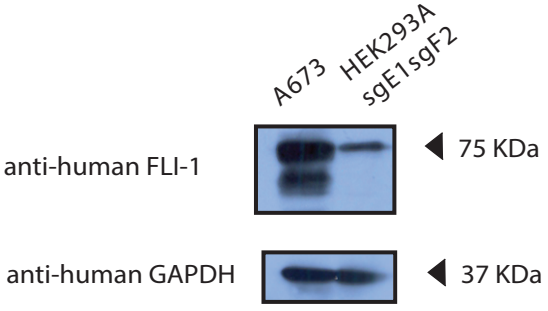
A673
HEK293A sgE1sgF2
anti-human FLI-1
75 KDa
anti-human GAPDH
37 KDa

A

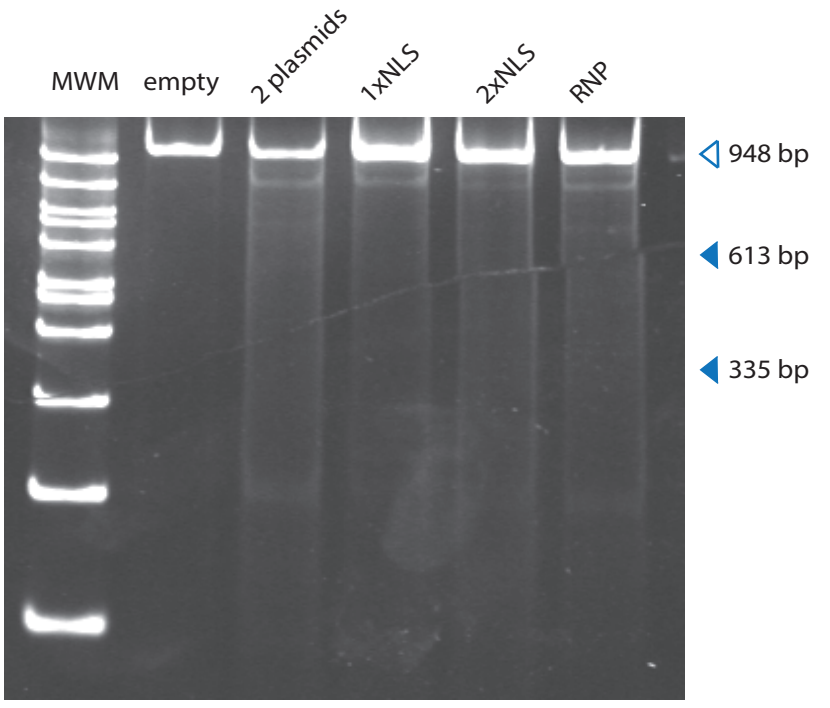

EWSR1 Off-target 1
(chromosome 14: -83517253)
AAaTTGTTTTTAGTtTGCCT aaG

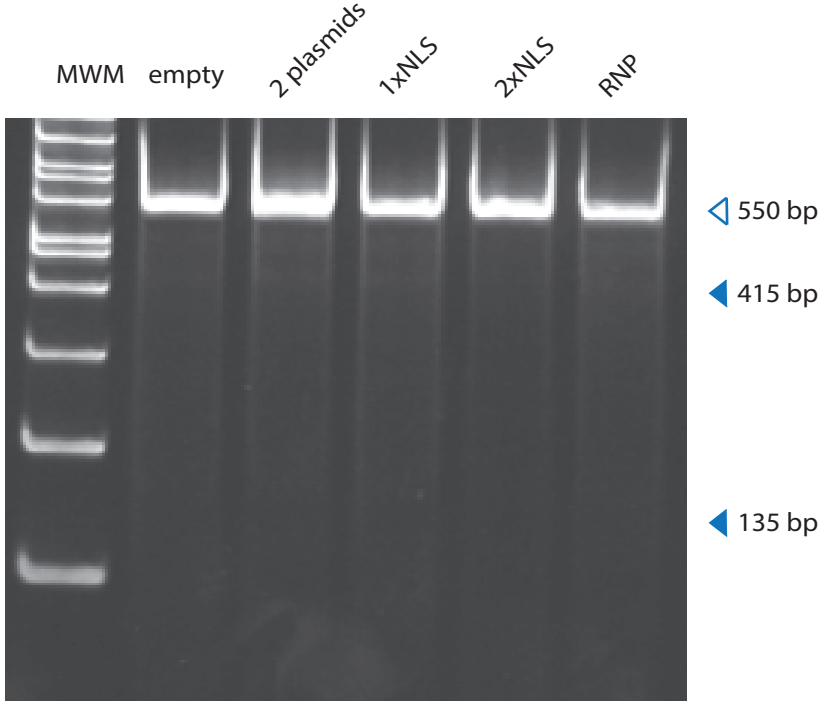

EWSR1 Off-target 2
(chromosome 14: 71328829)
AATTaGgaTTTAGTATGCCT aaG

B

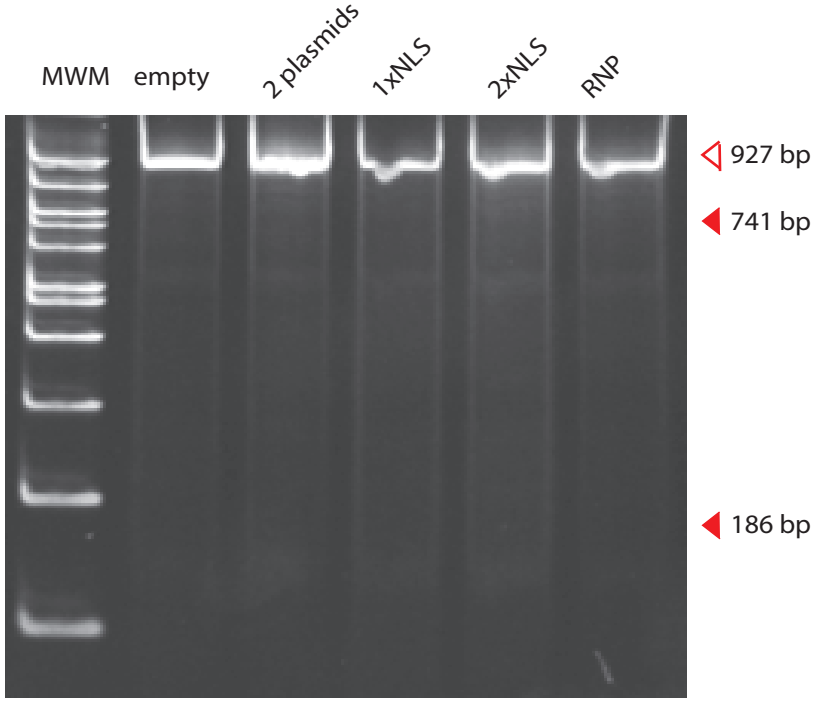

FLI1 Off-target 1
(chromosome 6: +155480)
CcaGCCTGGGCGATAGACCa caG

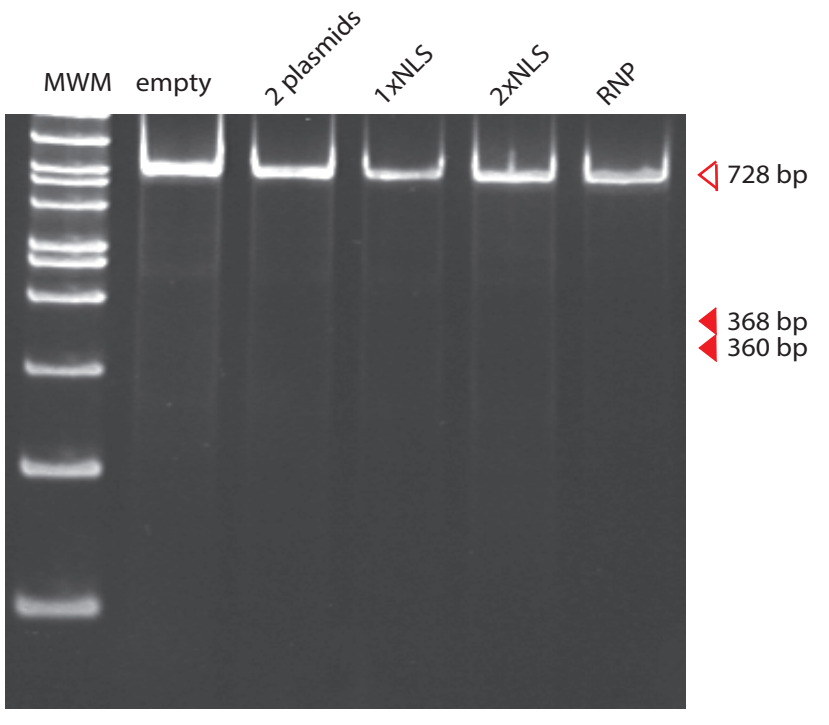

FLI1 Off-target 2
(chromosome 18: -63518093)
CcaGCCTGGGCGATAGACtG AGG

A

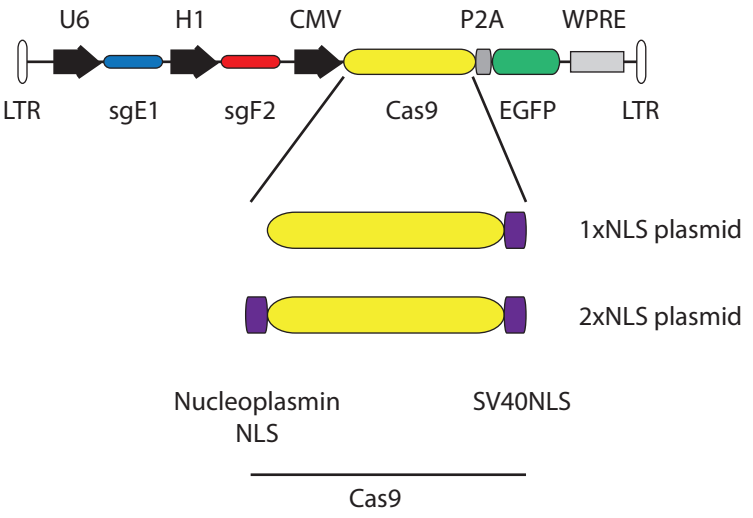

B

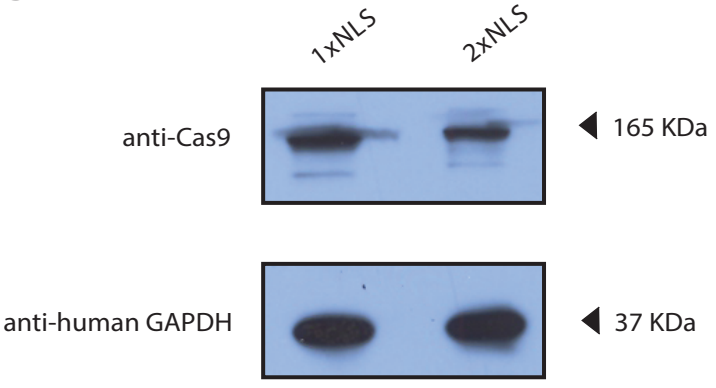

C

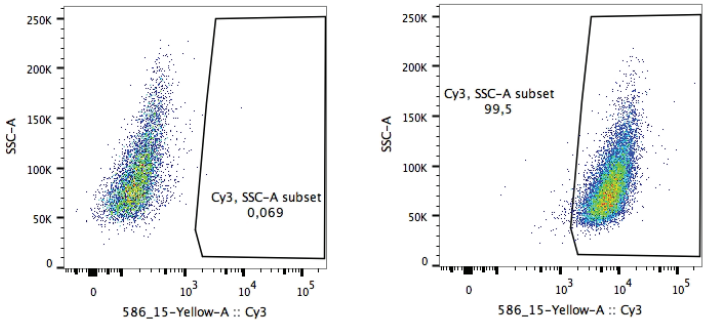

hiPSC negative control

hiPSC electroporated Cy3

A

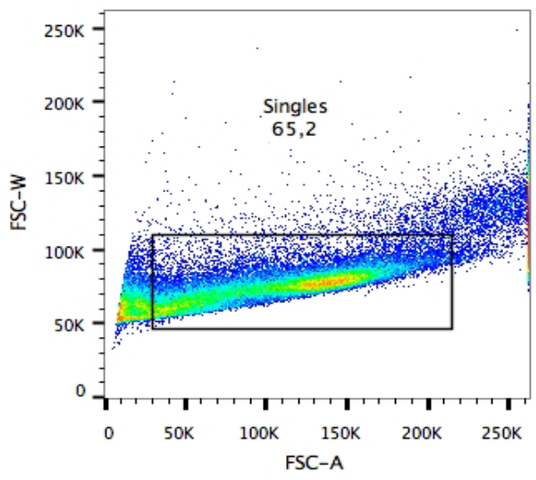
Singles
65,2
FSC-W
FSC-A

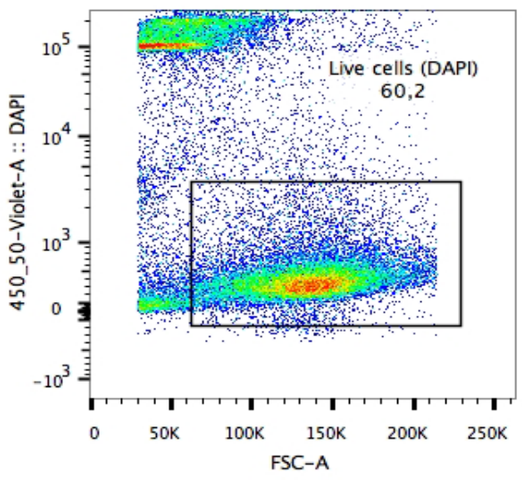
Live cells (DAPI)
60,2
450_50-Violet-A :: DAPI
FSC-A

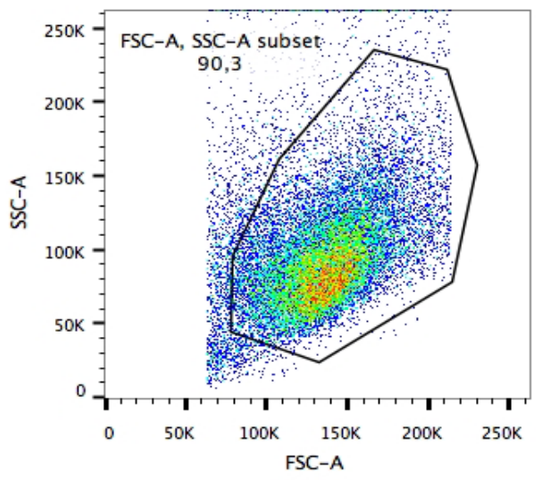
FSC-A, SSC-A subset
90,3
SSC-A
FSC-A

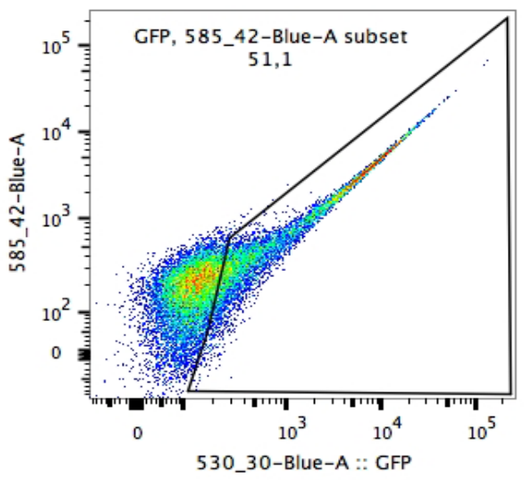
GFP, 585_42-Blue-A subset
51,1
585_42-Blue-A
530_30-Blue-A :: GFP

B

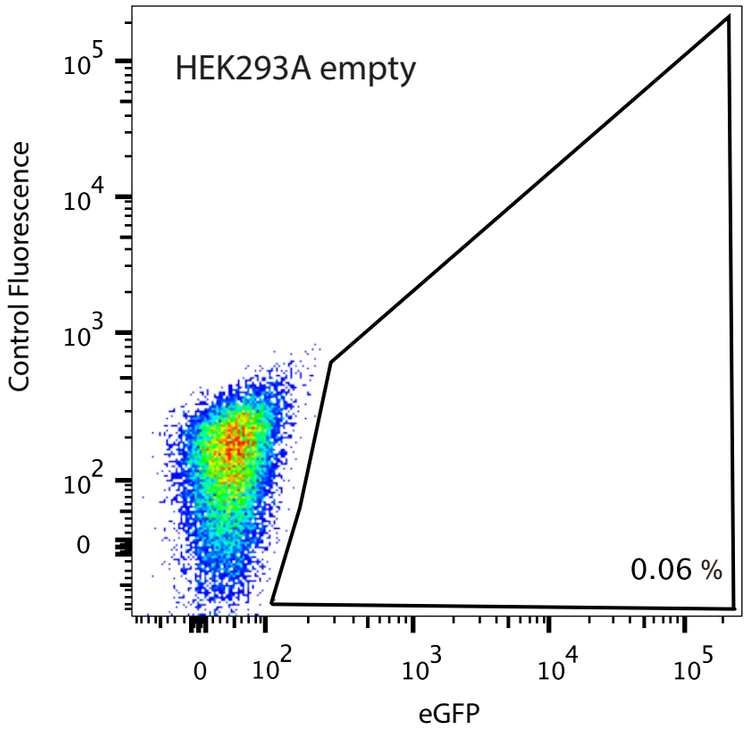
HEK293A empty
0.06 %
Control Fluorescence
eGFP

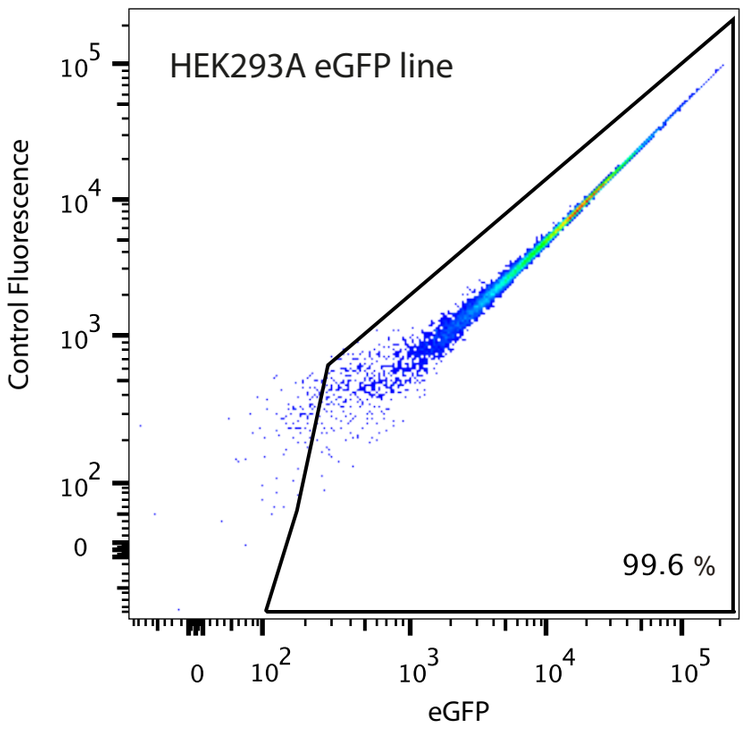
HEK293A eGFP line
99.6 %
Control Fluorescence
eGFP

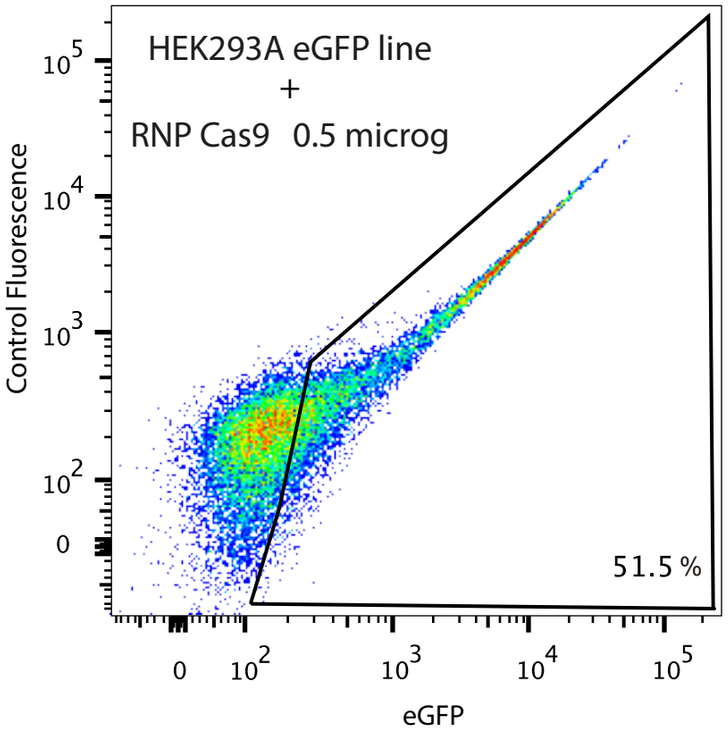
HEK293A eGFP line
+
RNP Cas9 0.5 microg
51.5 %
Control Fluorescence
eGFP

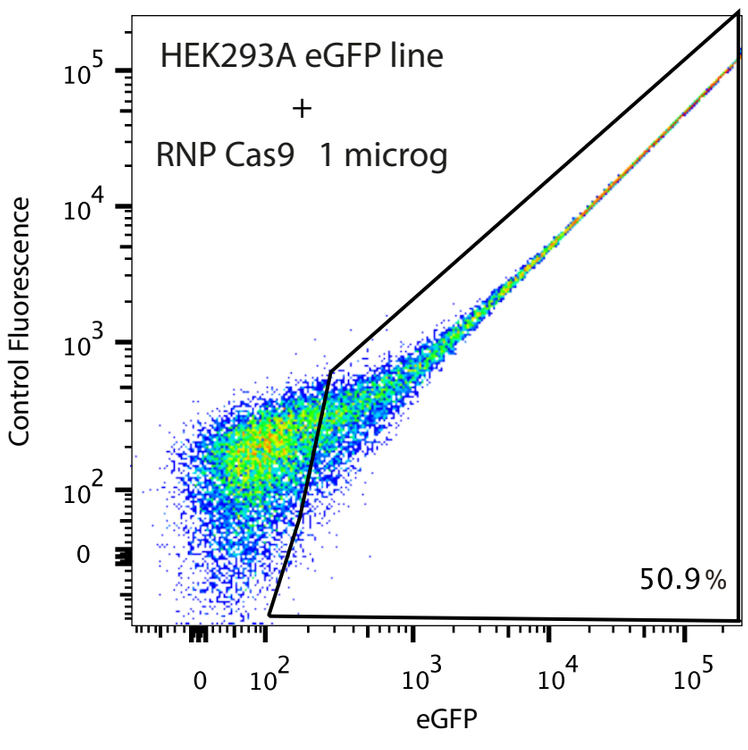
HEK293A eGFP line
+
RNP Cas9 1 microg
50.9 %
Control Fluorescence
eGFP

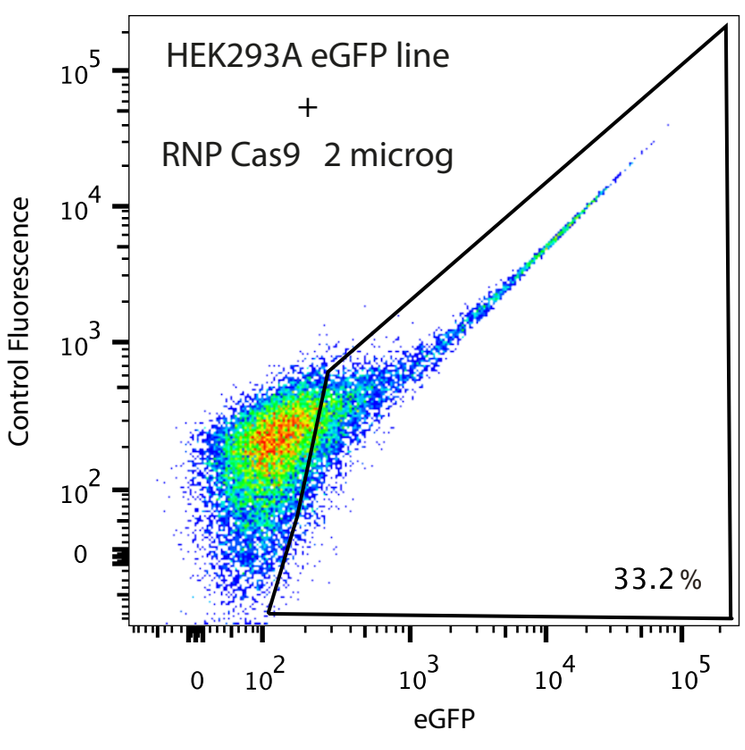
HEK293A eGFP line
+
RNP Cas9 2 microg
33.2 %
Control Fluorescence
eGFP

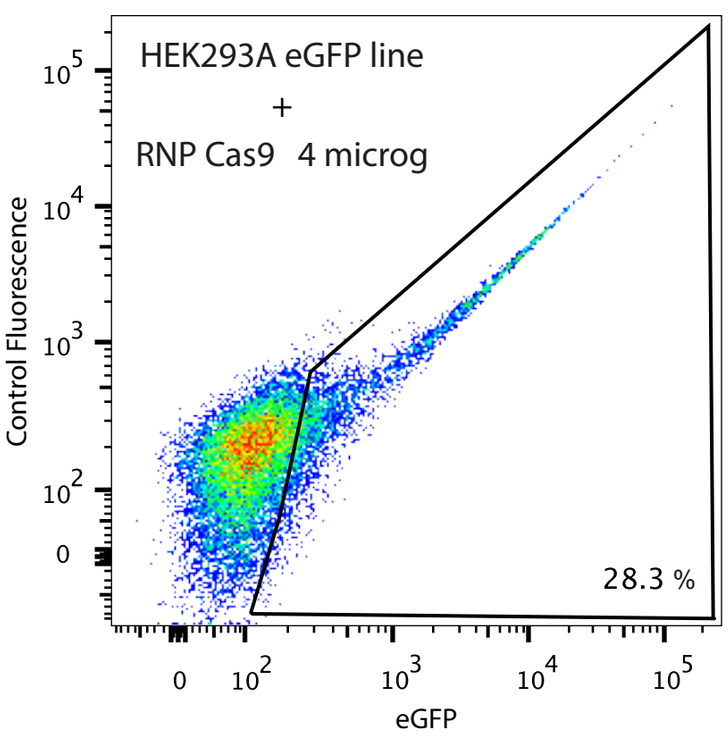
HEK293A eGFP line
+
RNP Cas9 4 microg
28.3 %
Control Fluorescence
eGFP

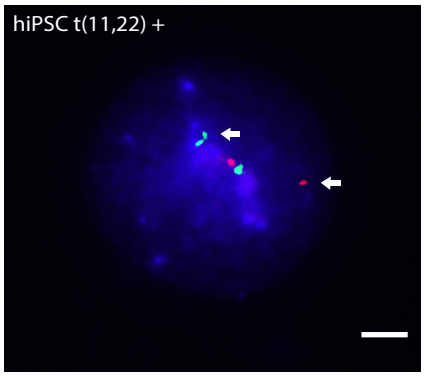
hiPSC t(11,22) +

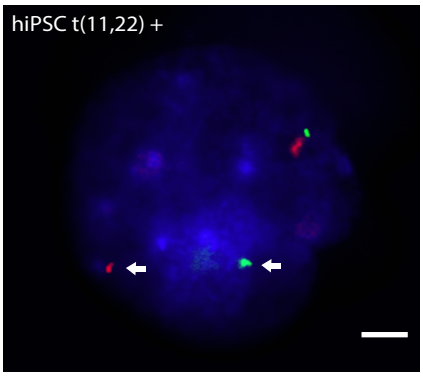
hiPSC t(11,22) +

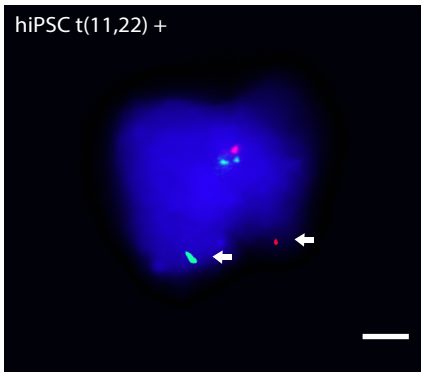
hiPSC t(11,22) +

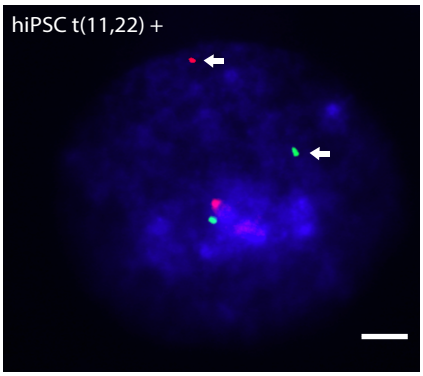
hiPSC t(11,22) +

Figure S1. Flow cytometry analysis of eGFP expression achieved with different delivery systems in HEK293A cells and hMSCs. Representative eGFP flow cytometry profiles showing the transfection efficiency achieved with five distinct delivery approaches in HEK293A cells (A) and hMSCs (B). Non-transfected cells were used as negative controls. IDLV: Integrative Defective Lentivirus, LV: Lentivirus.

Figure S2. (A) Agarose-gel electrophoresis of translocation-specific PCR products from pooled HEK293 and hMSCs samples corresponding to the *FLI1-EWSR1* fusion gene mapped at der(11) chromosome. (B) Representative agarose-gel electrophoresis of EWSR1-FLI1 and FLI1-EWSR1 RT-PCR products confirming the expression of both derivative fusion genes *EWSR1-FLI1* and *FLI1-EWSR1.* Sanger sequencing chromatograms showing the breakpoint region in the fusion genes mapped at der(11) and der(22) in HEK293 cells. (C) Representative Western blot analysis of EWSR1-FLI1 chimeric protein in A673 Ewing sarcoma cell line and HEK293 cells. GAPDH was used as a loading control.

Figure S3. Off-target effects in HEK293A cells produced with different CRISPR approaches. Representative T7 endonuclease I cleavage assay in HEK293A cells after electroporation with the 2-plasmid, 1xNLS, 2xNLS, or RNP approaches. Non-electroporated cells are used as controls. Full-length PCR products are indicated by an open triangle; predicted positions of digestion products are indicated by filled triangles.

Figure S4. (A) Schematic representation of 1xNLS and 2xNLS versions of pLV-U6#1H1#2-C9G. (B) Representative Western blot analysis of Cas9 protein in HEK293 cells transfected with either 1xNLS or 2xNLS versions of pLV-U6#1H1#2-C9G. GAPDH was used as a loading control. (C) Representative flow cytometry analysis of Cy3 signals in hiPSCs transfected with a synthetic Cy3 labelled oligonucleotide.

Figure S5. (A) Representative gating strategy to remove clumps or doublets, dead cells and debris or other events of non-interest from the data set while preserving cells based on size and or complexity. This gating strategy was used in Figures S1 and S5. (B) Flow cytometry analysis of eGFP expression in HEK293A cells after nucleofection with increasing amounts of RNPs.

Figure S6. Representative FISH images showing t(11;22)+ hiPSC after 8 weeks in culture. Arrows indicate separated signals corresponding to the der(22) and der(11) breakpoint regions. Interphase nuclei are counterstained with DAPI. Scale bars, 10 μm.

2 plasmids vs 1 plasmid

			assay #1			assay #2			assay #3			assay #4			total					
			positive	total	%	positive	total	%	positive	total	%	positive	total	%	positive	total	average	SD	p-value	
293 cells	2 plasmid	E1 + F2	1	400	0.25	2	400	0.50	1	285	0.35	4	566	0.71	8	1651	0.48	0.20	0.0090	**
	1 plasmid	E1F2	3	400	0.75	4	400	1.00	4	300	1.33	6	531	1.13	17	1631	1.04	0.24		

			assay #1			assay #2			assay #3			assay #4			total					
			positive	total	%	positive	total	%	positive	total	%	positive	total	%	positive	total	average	SD	p-value	
	2 plasmid	E1 + F2	0	450	0.00	1	500	0.20	1	471	0.21	1	431	0.23	2	1852	0.11	0.11		
hMSC cells					0.67			0.60							13	1904			0.0006	***
	1 plasmid	E1F2	3	450		3	500		4	467	0.86	3	487	0.62			0.68	0.12		

Delivery method

		assay #1			assay #2			assay #3			total				p-value		
	Compound	positive	total counted	%	positive	total counted	%	positive	total counted	%	positive	total counted	average	SD			
293 cells	Calcium Phos	3	242	1.24	3	256	1.17	2	205	0.98	8	703	1.14	0.14	C.P	0.0030	**
	Neon	6	245	2.45	5	225	2.22	5	185	2.70	16	655	2.44	0.24	Neon		
	LV	8	220	3.64	9	243	3.70	6	197	3.05	23	660	3.48	0.36	Neon	0.0210	ns
	IDLV	1	223	0.45	0	210	0.00	0	187	0.00	1	620	0.16	0.26	LV		
	L3000	4	257	1.56	5	238	2.10	3	221	1.36	12	716	1.68	0.38	LV	0.0004	***
															IDLV		
															C.P.	0.0099	**
															IDLV		
															C.P.	0.1225	ns
															L3000		

		assay #1			assay #2			assay #3			total				p-value		
	Compound	positive	total counted	%	positive	total counted	%	positive	total counted	%	positive	total counted	average	SD			
	Calcium Phos	0	387	0.00	0	264	0.00	0	431	0.00	0	1082	0.00	0.00	L3000	0.9788	ns
	Neon	3	311	0.96	4	300	1.33	3	238	1.26	10	849	1.18	0.20	Neon		
hMSC cells	LV	5	227	2.20	7	219	3.20	5	209	2.39	17	655	2.59	0.53	Neon	0.0315	**
	IDLV	1	341	0.29	0	223	0.00	1	500	0.20	2	1064	0.19	0.15	LV		
	L3000	3	215	1.39	3	298	1.01	4	350	1.14	10	863	1.16	0.20	LV	0.0110	**
															IDLV		
															L3000	0.0027	***
															IDLV		
															C.P.	0.0092	**
															L3000		

Sorting

		assay #1			assay #2			assay #3			total				p-value		
		positive	total counted	%	positive	total counted	%	positive	total counted	%	positive	total counted	average	SD			
293 cells	Non Sorted	2	306	0.65	2	311	0.64	3	294	1.02	7	911	0.77	0.22	Non sorted / Low	0.3488	ns
	Sorted Low	1	299	0.33	3	315	0.95	0	268	0.00	4	882	0.45	0.48			
	Sorted High	5	273	1.83	5	303	1.65	4	233	1.72	14	809	1.73	0.09	Low / High	0.0387	*
															Non sorted / High	0.0080	**

		assay #1			assay #2			assay #3			total				p-value	
		positive	total counted	%	positive	total counted	%	positive	total counted	%	positive	total counted	average	SD		
hMSC cells	Non Sorted	1	312	0.32	0	325	0.00	1	294	0.34	2	931	0.22	0.19	0.0145	*
	Sorted	2	283	0.71	3	315	0.95	2	247	0.81	7	845	0.83	0.12		

1xNLS vs 2xNLS

		assay #1			assay #2			assay #3			total				p-value		
		positive	total counted	%	positive	total counted	%	positive	total counted	%	positive	total counted	average	SD			
293 cells	1xNLS	3	515	0.58	1	516	0.19	4	557	0.72	8	1588	0.50	0.27	1xNLS / 2xNLS	0.0899	ns
	2xNLS	9	480	1.88	5	532	0.94	18	737	2.44	32	1749	1.83	0.76			ns

		assay #1			assay #2			assay #3			total				p-value		
		positive	total counted	%	positive	total counted	%	positive	total counted	%	positive	total counted	average	SD			
hMSC cells	1xNLS	1	545	0.18	0	527	0.00	0	501	0.00	1	1573	0.06	0.11	1xNLS / 2xNLS	0.0145	*
	2xNLS	2	495	0.40	2	543	0.37	3	500	0.60	7	1538	0.46	0.13			

ssODNs

293 cells

ssODN	assay #1 positive	assay #1 total counted	assay #1 %	assay #2 positive	assay #2 total counted	assay #2 %	assay #3 positive	assay #3 total counted	assay #3 %	total positive	total total counted	average	SD
60	1	304	0.33	1	300	0.33	1	297	0.34	3	901	0.33	0.01
90	1	347	0.29	1	260	0.38	1	308	0.32	3	915	0.33	0.05
120	2	301	0.66	1	300	0.33	2	310	0.65	5	911	0.55	0.19
150	4	310	1.29	3	300	1.00	3	290	1.04	10	900	1.11	0.16
180	2	346	0.58	2	305	0.66	1	280	0.36	5	931	0.54	0.15
no ssODN	1	302	0.33	0	300	0.00	0	315	0.00	1	917	0.11	0.19

p-value		
60	0.1812	ns
empty		
90	0.1757	ns
empty		
120	0.0469	*
empty		
150	0.0025	**
empty		
180	0.0440	*
empty		

293 cells

ssODN	assay #1 positive	assay #1 total counted	assay #1 %	assay #2 positive	assay #2 total counted	assay #2 %	assay #3 positive	assay #3 total counted	assay #3 %	total positive	total total counted	average	SD
e1f2	5	323	1.55	4	276	1.45	5	290	1.72	14	889	1.57	0.14
f1e2	2	194	1.03	2	220	0.91	4	234	1.71	8	648	1.24	0.43
e1f2 + f1e2	4	198	2.02	5	263	1.90	5	231	2.16	14	692	2.02	0.13
no ssODN	1	194	0.52	1	212	0.47	1	305	0.33	3	711	0.42	0.10

p-value		
e1f2	0.0006	***
empty		
f1e2	0.0822	ns
empty		
e1f2 + f1e2	0.0058	**
empty		

hMSC cells

ssODN	assay #1 positive	assay #1 total counted	assay #1 %	assay #2 positive	assay #2 total counted	assay #2 %	assay #3 positive	assay #3 total counted	assay #3 %	total positive	total total counted	average	SD
e1f2	NA	NA		NA	NA		NA	NA		NA	NA		
f1e2	NA	NA		NA	NA		NA	NA		NA	NA		
e1f2 + f1e2	7	306	2.29	8	250	3.20	10	382	2.62	25	938	2.67	0.46
no ssODN	1	500	0.20	0	300	0.00	2	315	0.64	3	1115	0.27	0.32

p-value		
NA	NA	
NA		
e1f2 + f1e2	0.0027	**
empty		

NA: Not Applicable

DNA-end processing factors

293 cells

Factors	assay #1 positive	assay #1 total counted	assay #1 %	assay #2 positive	assay #2 total counted	assay #2 %	assay #3 positive	assay #3 total counted	assay #3 %	total positive	total total counted	average	SD
empty	8	284	2.82	6	249	2.41	7	261	2.68	21	794	2.64	0.21
AICDA	5	352	1.42	4	294	1.36	5	308	1.62	14	954	1.47	0.14
ARTEMIS	10	307	3.26	9	273	3.30	9	281	3.20	28	861	3.25	0.05
PARP1	9	304	2.96	3	297	1.01	6	285	2.10	18	886	2.03	0.98
TREX2	9	273	3.30	11	287	3.83	8	268	2.99	28	828	3.38	0.43
DCLREI	8	280	2.86	7	257	2.72	6	241	2.49	21	778	2.70	0.19
FEN1	7	292	2.40	6	237	2.53	4	189	2.12	17	718	2.37	0.21
MRE11	7	225	3.11	11	308	3.57	8	271	2.95	26	804	3.23	0.32

p-value		
AICDA / empty	0.0022	**
ARTEMIS / empty	0.0306	*
PARP1 / empty	0.3928	ns
TREX2 / empty	0.0786	ns
DCLREI / empty	0.7542	ns
FEN1 / empty	0.1682	ns
MRE11 / empty	0.0701	ns

AICDA & ARTEMIS has a significant p-value but with a decreasing translocation efficiency

hMSC cells

Factors	assay #1 positive	assay #1 total counted	assay #1 %	assay #2 positive	assay #2 total counted	assay #2 %	assay #3 positive	assay #3 total counted	assay #3 %	total positive	total total counted	average	SD
empty	1	315	0.32	1	301	0.33	1	289	0.35	3	905	0.33	0.01
AICDA	na	na	na	na	na	na	na	na	na	na	na	na	na
ARTEMIS	0	321	0.00	1	356	0.28	0	294	0.00	1	971	0.10	0.16
PARP1	2	321	0.62	3	362	0.83	2	278	0.72	7	961	0.73	0.10
TREX2	2	301	0.66	3	387	0.77	2	291	0.69	7	979	0.72	0.06
DCLREI	na	na	na	na	na	na	na	na	na	na	na	na	na
FEN1	na	na	na	na	na	na	na	na	na	na	na	na	na
MRE11	na	na	na	na	na	na	na	na	na	na	na	na	na

p-value		
ARTEMIS / empty	0.1248	ns
PARP1 / empty	0.0206	*
TREX2 / empty	0.0056	**

RNP Cas9

		assay #1			assay #2			assay #3			total				p-value		
		positive	total counted	%	positive	total counted	%	positive	total counted	%	positive	total counted	average	SD			
293 cells	2 plasmids	0	213	0.00	1	200	0.50	2	353	0.57	3	766	0.39	0.31	2NLS / 2 plasmids	0.0253	*
	2NLS	4	301	1.33	2	204	0.98	4	328	1.22	10	833	1.20	0.18			
	RNP	6	203	2.96	9	258	3.49	11	250	4.40	26	711	3.66	0.73	RNP / 2 plasmids	0.0081	**

		assay #1			assay #2			assay #3			total				p-value		
		positive	total counted	%	positive	total counted	%	positive	total counted	%	positive	total counted	average	SD			
hMSC cells	2NLS plasmid	0	335	0.00	0	427	0.00	1	468	0.21	1	1230	0.08	0.12	RNP / Cas9 plasmid	0.0007	***
	RNP	3	327	0.92	4	418	0.96	4	350	1.14	11	1095	1.00	0.12			

		assay #1			assay #2			assay #3			total				p-value		
		positive	total counted	%	positive	total counted	%	positive	total counted	%	positive	total counted	average	SD			
	RNP	4	427	0.94	3	400	0.75	3	368	0.82	10	1195	0.84	0.09	RNP / RNP + TREX2	0.9700	ns
hMSC cells	RNP + TREX2	4	413	0.97	3	408	0.74	3	381	0.79	10	1202	0.83	0.12			
	RNP + PARP1	3	397	0.76	2	400	0.50	4	376	1.06	9	1173	0.77	0.28	RNP / RNP + PARP1	0.7517	ns
	RNP + ssODN	6	385	1.56	7	403	1.74	6	363	1.65	19	1151	1.65	0.09			
															RNP / RNP + TREX2	0.0004	***

		assay #1			assay #2			assay #3			total				p-value		
		positive	total counted	%	positive	total counted	%	positive	total counted	%	positive	total counted	average	SD			
hiPSC	RNP + ssODN	3	261	1.15	6	417	1,.44	6	398	1.51	15	1076	1.39	0.19	0.0033	**	
	2NLS plasmid	1	353	0.28	2	461	0.44	2	375	0.53	5	1189	0.42	0.13			

TORRES-RUIZ et al. Sup. Table. 2

Name	Application	Sequence
OTf2 Fw	*FLI1* off target	GGAGTGCATGGGAGTTGAGT
OTf2 Rv	*FLI1* off target	GCAGAGGAAGTGAGAAGCGT
OTf4 Fw	*FLI1* off target	CATGTAGCGAGGGTAGCAGG
OTf4 Rv	*FLI1* off target	CTAACTGTGTGGCTGGGGAC
OTe1 Fw	*EWSR1* off target	TGCTTTCCAGCCCTAGAGGA
OTe1 Rv	*EWSR1* off target	TGCTCACGTTTGCCATGAGA
OTe7 Fw	*EWSR1* off target	TGCATAAGGGACAGAGCAACA
OTe7 Rv	*EWSR1* off target	TTTGAGTGACCCCCGAGTTT
EWSR1 Rv	*EWSR1* on-target	GCTGCCTCCCCACTTTACAT
EWSR1 Fw1	*EWSR1* on-target	AGGCTGGTCTCGAACTCCTG
FLI1 Rv1	*FLI1* on-target	TGGATGCCTTTGAACCAAT
FLI1 Fw	*FLI1* on-target	ATGCAAGGAGGACTGTGAT
EWSR1 Fw2	Tranlocation detection	AGGACACATCTTTAGGGCA
FLI1 Rv2	Tranlocation detection	GCGTGGTGATAGGTTTGGCT
ssODN_e1f2 60	ODN	agtgctttttttccaatttgtttttagtatgccgaggctctgtcttcagaggaaaaaaggt
ssODN_e1f2 90	ODN	cccagtgaagatttcagtgctttttttccaatttgtttttagtatgccgaggctctgtcttcagaggaaaaaaggttgcccccttgtggac
ssODN_e1f2 120	ODN	taacatcttggatgccccagtgaagatttcagtgctttttttccaatttgtttttagtatgccgaggctctgtcttcagaggaaaaaaggttgcccccttgtggacaactatctacagtac
ssODN_e1f2 150	ODN	gcatggcattccagctaacatcttggatgccccagtgaagatttcagtgctttttttccaatttgtttttagtatgccgaggctctgtcttcagaggaaaaaaggttgcccccttgtggacaactatctacagtacccattttgaagctga
ssODN_e1f2 180	ODN	ggacacatctttagggcatggcattccagctaacatcttggatgccccagtgaagatttcagtgctttttttccaatttgtttttagtatgccgaggctctgtcttcagaggaaaaaaggttgcccccttgtggacaactatctacagtacccattttgaagctgaacccactgaggccca
sg*EWSR1*_1	single-guide sequence	AATTTGTTTTTAGTATGCCT **TGG**
sg*FLI1*_2	single-guide sequence	CTGGCCTGGGCGATAGACCG **AGG**

Table S1: Details of the FISH results included in this study.

Table S2: Oligonucleotide, ssODN, and sgRNA sequences used in this study.

SUPPLEMENTARY EXPERIMENTAL PROCEDURES

Transfection and Electroporation

Cells were transfected with endotoxin-free DNA (Qiagen) in 6-well plates. Calcium-phosphate-based transfection was performed as previously described (Torres et al., 2014a). Briefly, HEK293A cells were seeded and grown to confluence, and then transfections were performed with 6 µg plasmid DNA mixed with $CaCl_2$. After 48-72 hours, cells were processed for subsequent analysis. For electroporation, the Neon Transfection System was used (Thermo Fisher Sci). Confluent hMSCs, hiPSCs and HEK293A cells were trypsinized, resuspended in R solution, and electroporated using the following conditions. For hMSCs, 10-µl tips were used to electroporate 1×10^5 cells with a single 40-ms pulse of 990 V. For HEK293A cells, 4×10^5 cells were electroporated with 10-µl tips using three 10-ms pulses of 1245 V. Finally, hiPSCs were electroporated with 10-µl tips using 2×10^5 cells with three 5-ms pulses of 1400 V. After electroporation, cells were seeded in a 24-well plate containing pre-warmed medium. When required, cells were sorted 72 h post-transfection. For co-transfection experiments, 200 pmol of ssODN (IDT) or end processing plasmids were included.

Immunofluorescence

Immunofluorescence was carried out as previously described, with modifications (Torres and Ramirez, 2009). Briefly, after nucleofection, cells were seeded onto 8-well glass bottom µ-Slides (Ibidi). After 72 h, cells were washed twice with PBS and fixed 10 min in 4% paraformaldehyde, permeabilized with 0.5% TritonX-100/PBS, and blocked with 4% normal goat serum. For Cas9 studies, samples were incubated overnight at 4ºC with anti-Cas9 antibody (1/500 dilution, 7A9-3A3, Active Motif) and then for 1 h at RT with Alexa-fluor-555 secondary antibody (dilution 1/1000, Molecular Probes). For pluripotency-associated markers, hiPSCs were incubated overnight at 4ºC with anti-OCT4 (1/500 dilutions, Cell Signaling Tech) or anti-SSEA4 antibodies (1/500 dilutions, MC-813-70, StemCell Tech) and then 1h at RT with Alexa-fluor-555 and Alexa-fluor-647 secondary antibodies in the darkness. Nuclei were counterstained with DAPI, and samples air-dried and mounted in gelatin (Sigma Aldrich). Images were captured with a Leica SP5 confocal laser-scanning microscope.

Genomic DNA Extraction and PCR Analysis

Genomic DNA was extracted using standard procedures. Briefly, $5\text{-}10\times10^6$ cells were either trypsinized or scraped, washed in PBS, pelleted, and lysed in 100 mM NaCl, Tris (pH 8.0) 50 mM, EDTA 100 mM, and 1% SDS. After overnight digestion at 56ºC with 0.5 mg/ml of proteinase K (Roche), DNA was cleaned by precipitation with saturated NaCl, and the clear supernatant was precipitated with isopropanol, washed with 70% ethanol, air-dried, and resuspended overnight at

RT in 1xTE buffer. Serial DNA dilutions were quantified with a NanoDrop 1000 Spectrophotometer (Thermo Scientific). Standard PCR was performed under the following conditions: denaturation at 95°C for 1 min followed by 30 cycles of denaturation at 94°C for 30 s, annealing at 62.5°C for 30 s, extension at 72°C for 60 s, and a final extension of 5 min at 72°C. Primers used are listed in **Table S1**.

Lentivirus Generation, Titration, and Transduction

Viruses were produced by transient plasmid transfection into HEK293T cells using the calcium phosphate method (Torres et al., 2011). Briefly, cells were seeded at 1.1×10^7 cells/dish in 15-cm dishes the day before transfection. Cells were transfected using calcium phosphate with 3 µg pRSV-Rev, 3.75 µg pMD.2G (VSV-G), 13 µg pMDLg/pRRE (or 13 µg pMDLg/pD64VRRE for production of non-integrative lentiviral vectors), and 35 µg of transfer plasmid (pLVX-U6-sgRNA$^{\#1}$-H1-sgRNA$^{\#2}$-Cas9-2A-eGFP). The medium was collected after 48 h, cleared by low-speed centrifugation, and filtered through 0.45-µm pore PVDF filters (Millipore). Viral stocks were concentrated by ultracentrifugation at 20,000 rpm for 2 h at 16ºC. Pellets containing lentivirus were air-dried and resuspended overnight at 4ºC in 400 µl of medium. Viral titers in HEK293T cells transduced with vectors expressing fluorescent proteins were determined by FACS analysis (transduction units/ml). In the absence of a fluorescent reporter, titer was estimated by qPCR of particles in supernatants (particles/ml). Values ranged from 10^7 to 10^8 TU/ml and were at a TU/particle ratio of 1:100. Cells were transduced at different multiplicities of infection in medium containing Polybrene (8 µg/ml final concentration). Cells were incubated at 37ºC for 6 h, and the viral supernatant was then replaced with fresh medium and analysed 72 h later.